

EMPIRICAL PARTIAL WAVE ANALYSIS OF $\pi+p$ ELASTIC SCATTERING
ABOVE 1 GeV/c*

Martin L. Perl and Mary C. Corey
Stanford Linear Accelerator Center
Stanford University
Stanford, California

(Submitted to Physical Review)

*Supported in part by the U.S. Atomic Energy Commission and
in part by the U.S. Office of Naval Research.

ABSTRACT

The partial wave equation

$$d\sigma/d\Omega = \left| [1/2ik] \sum_{\ell=0}^L (2\ell + 1)(1 - a_{\ell}) P_{\ell}(\cos \theta) \right|^2$$

has been used to fit most of the recent $\pi+p$ differential cross section measurements above 1 GeV/c. The a_{ℓ} were determined by the method of weighted least squares, with the further requirement that they be real and they satisfy either constraints of the form $1 \geq 1 - a_{\ell} \geq 0$ (which allows the scattering to be interpreted as purely absorptive) or the more relaxed constraints $2 \geq 1 - a_{\ell} \geq 0$. This equation with the requirements does not allow the scattering amplitude to have a spin-flip part or a real part, but for one set of data further terms were added to allow these additional parts of the scattering amplitude. For each differential cross section at the various energies, a set of a_{ℓ} values was determined which in almost all cases fit the measured cross sections quite well. These sets of a_{ℓ} parameters have two properties in common. First, all a_{ℓ} except a_0 satisfy $1 \geq 1 - a_{\ell} \geq 0$. The a_0 parameters (s-wave amplitudes) required $1 - a_0 \geq 1$ except for the higher energies where $1 \geq 1 - a_0 \geq 0$ was obtained. Second, graphs of $1 - a_{\ell}$ versus ℓ (one graph for each different cross section measurement) show that $1 - a_{\ell}$ decreases rather smoothly with increasing ℓ and that the slope is roughly either linear or concave upward. No striking variations in the a_{ℓ} parameters are observed when the energy is close to one of the $\pi+p$ total cross section resonances. The a_{ℓ} parameters are

interpreted using $1 - a_l$ as a measure of the absorption of the l -th partial wave by inelastic processes. Differential cross section measurements of π^-+p at 2.01 GeV/c and of π^++p at 2.02 GeV/c previously published only in graphical form are given in the appendix.

I. INTRODUCTION

In the last few years a large amount of data on elementary particle elastic scattering above 1 GeV/c has been produced.¹ Most of it has been analyzed from the standpoint of the simpler form of the Regge theory of elastic scattering in which the data was to be fitted with only a few parameters, some of these parameters having physical significance.^{2,3} The hope that such a simple theory would be satisfactory has not been fulfilled. More parameters were required than first thought necessary,^{4,5,10,15} and the theory was found to be much more complex than first supposed. Therefore, it is desirable to look at this recent data from some other theoretical viewpoint. Ideally one would like a theory of elastic scattering derived from a general form of quantum field theory or S-matrix theory, this theory at the same time containing only a few parameters to be determined by experiment. It would be even more satisfactory if at some level the theory, or its parameters, had direct physical significance or gave some physical insight. No such theory exists and, therefore, we have turned back to some older concepts which while not directly related to any profound theory at least provide a way of fitting the data so that the values of parameters provide physical insight. These concepts are the partial wave analysis of scattering theory combined with the assumption that at high incident momenta, most of the elastic scattering is absorptive.

We have analyzed the π^+p elastic scattering above 1 GeV/c using empirical partial wave amplitudes with two purposes in mind. First, looking upon this analysis as a generalization of the optical

model, we wished to discover how well a generalized optical model could fit not only the diffraction peak part of the elastic scattering, but also the entire differential cross section.

Secondly, the resonances recently discovered above 1 GeV/c in $\pi+p$ total cross sections are sometimes related to a particular angular momentum state, whose identity is sought by studying the elastic differential cross section at the resonance energies. Thus, the large peak in the back hemisphere in π^+p elastic scattering at 1.5 GeV/c has been related by both V. Cook et al.⁶ and J. Helland⁷ to the $\pi+p$ total cross section maximum at 1.4 GeV/c; and the second peak in the π^-p differential cross section at 2.02 GeV/c has been related by Damouth et al.⁸ to the 2.1 GeV/c π^-p total cross section maximum. However, L. M. Simmons⁹ has shown that this second peak in π^-p differential cross section at 2.07 GeV/c can be explained by a simple optical model. We have investigated this point further.

In this paper the analysis is almost completely restricted to purely absorptive scattering; that is, we usually neglect the effects of non-absorptive elastic scattering and spin-flip elastic scattering. Originally we intended to include these effects, but as will be described later the fitting problem becomes very complex when these effects are included, and we have found no solution to the problem.

II. THEORY AND METHOD OF ANALYSIS

A general discussion of theories of elastic scattering has been given by Perl, Jones, and Ting¹⁰ and the reader is referred to that paper and its references for the background. We begin here immediately with the partial wave analysis of $\pi + p$ scattering. For spinless particles when no inelastic processes occur, Schiff¹¹ shows that the differential cross section in the barycentric system $d\sigma(\theta)/d\Omega$ is given by

$$d\sigma(\theta)/d\Omega = |A(\theta)|^2 \quad (1)$$

where

$$A(\theta) = [1/2ik] \sum_{\ell=0}^{\infty} (2\ell + 1) \left(\exp(2i\delta_{\ell}) - 1 \right) P_{\ell}(\cos \theta) \quad (2)$$

Here ℓ is the orbital angular momentum quantum number of the partial wave, k is the wave number in cm^{-1} in the barycentric system, θ is the scattering angle in the barycentric system, $P_{\ell}(\cos \theta)$ is normalized so that $P_{\ell}(1) = 1$, and δ_{ℓ} is the phase shift always taken to be $-\pi \leq \delta_{\ell} \leq \pi$. For the remainder of this paper all quantities will be in the barycentric system and $P_{\ell}(\cos \theta)$ will always be normalized as above.

If inelastic processes can occur, then Eq. (2) is modified by the addition of quantities a_{ℓ} where $0 \leq a_{\ell} \leq 1$ and

$$A(\theta) = [1/2ik] \sum_{\ell=0}^{\infty} (2\ell + 1) \left(a_{\ell} \exp(2i\delta_{\ell}) - 1 \right) P_{\ell}(\cos \theta). \quad (3)$$

If there are no inelastic processes in the ℓ -th wave, then $a_\ell = 1$; if the ℓ -th wave is completely absorbed by inelastic process, then $a_\ell = 0$. Thus, a_ℓ is the degree of elasticity.

Finally, if one of the particles has spin 1/2 and the other spin 0, as in the π +p system, then for each ℓ there are two possible total angular momentum states $j = \ell \pm 1$; Eq. (3) becomes

$$A(\theta) = [1/2ik] \sum_{\ell=0}^{\infty} \left[(\ell + 1) (a_\ell^+ \exp(2i\delta_\ell^+) - 1) + \ell (a_\ell^- \exp(2i\delta_\ell^-) - 1) \right] P_\ell(\cos \theta) \quad (4)$$

But a second amplitude appears also, $B(\theta)$, where

$$B(\theta) = [1/2ik] \sum_{\ell=1}^{\infty} \left[a_\ell^+ \exp(2i\delta_\ell^+) - a_\ell^- \exp(2i\delta_\ell^-) \right] \sin \theta \left[dP_\ell(\cos \theta)/d(\cos \theta) \right] \quad (5)$$

and $d\sigma(\theta)/d\Omega$ is now given by

$$d\sigma(\theta)/d\Omega = |A(\theta)|^2 + |B(\theta)|^2 \quad (6)$$

This $B(\theta)$ results from that part of the elastic process in which the orientation of the spin of the proton is changed. $B(\theta)$ is referred to as the spin-flip amplitude in this paper.

Equation (4) may be rewritten

$$\begin{aligned}
 A(\theta) = [1/2ik] & \left\{ \sum_{\ell=0}^{\infty} [(\ell+1)(a_{\ell}^{+} \cos 2\delta_{\ell}^{+} - 1) + \ell(a_{\ell}^{-} \cos 2\delta_{\ell}^{-} - 1)] P_{\ell}(\cos \theta) \right. \\
 & \left. + i \sum_{\ell=0}^{\infty} [(\ell+1)(a_{\ell}^{+} \sin 2\delta_{\ell}^{+}) + \ell(a_{\ell}^{-} \sin 2\delta_{\ell}^{-})] P_{\ell}(\cos \theta) \right\} \\
 = A_i(\theta) & + A_r(\theta) . \tag{4a}
 \end{aligned}$$

If all δ_{ℓ}^{+} and δ_{ℓ}^{-} are zero then the real term $A_r(\theta)$ is zero and $A(\theta)$ is then referred to in this paper as purely absorptive. This name simply indicates that there is no phase shift of the partial waves, only absorption of them. When some δ_{ℓ}^{+} or δ_{ℓ}^{-} are not zero, then some non-absorptive scattering is said to be present. When this phrase non-absorptive is used, one should recall that it means not only that the real part $A_r(\theta)$ is non-zero but also that the imaginary part $A_i(\theta)$ is modified.

Just as $A(\theta)$ can be separated into real and imaginary parts, so can $B(\theta)$. Thus Eq. (6) is rewritten

$$d\sigma(\theta)/d\Omega = |A_i(\theta)|^2 + |A_r(\theta)|^2 + |B_i(\theta)|^2 + |B_r(\theta)|^2$$

where

$$\begin{aligned}
 A_i(\theta) &= [1/2ik] \sum_{\ell=0}^{\infty} [(\ell+1)(a_{\ell}^{+} \cos 2\delta_{\ell}^{+} - 1) + \ell(a_{\ell}^{-} \cos 2\delta_{\ell}^{-} - 1)] P_{\ell}(\cos \theta) \\
 A_r(\theta) &= [1/2k] \sum_{\ell=0}^{\infty} [(\ell+1)(a_{\ell}^{+} \sin 2\delta_{\ell}^{+}) + \ell(a_{\ell}^{-} \sin 2\delta_{\ell}^{-})] P_{\ell}(\cos \theta) \\
 B_i(\theta) &= [1/2ik] \sum_{\ell=0}^{\infty} [a_{\ell}^{+} \cos 2\delta_{\ell}^{+} - a_{\ell}^{-} \cos 2\delta_{\ell}^{-}] \sin \theta [dP_{\ell}(\cos \theta)/d(\cos \theta)] \\
 B_r(\theta) &= [1/2k] \sum_{\ell=0}^{\infty} [a_{\ell}^{+} \sin 2\delta_{\ell}^{+} - a_{\ell}^{-} \sin 2\delta_{\ell}^{-}] \sin \theta [dP_{\ell}(\cos \theta)/d(\cos \theta)]
 \end{aligned} \tag{6a}$$

Now the partial wave analysis is useful only if a small number of ℓ values contribute to the scattering. This has been the basis of its very extensive use at low energies for $\pi+p$ and $p+p$ scattering. However, for elementary particle scattering above 1 GeV/c, partial wave amplitudes at least through $\ell = 4$ must be used; and since for each ℓ value there are four numbers to be determined, at least twenty parameters should be determined. When one considers that the data is usually not of sufficient statistical accuracy to determine twenty parameters, that there are ambiguities, and that these are non-linear equations, it is clearly not possible simply to go ahead and evaluate these parameters without any restrictive assumptions.

In fact, it has been customary to make some very specific physical assumptions in order to solve this problem, and the most often used assumptions lead to the optical model. In this model one assumes that $\delta_{\ell}^{\pm} = 0$ and that $a_{\ell}^{+} = a_{\ell}^{-}$. In the simplest case of the optical model one goes further and sets

$$\left. \begin{array}{l} a_{\ell} = a < 1, \quad 0 \leq \ell \leq L \\ a_{\ell} = 1, \quad \ell > L \end{array} \right\} \text{where } L \gg 1 \quad (7)$$

which leads to the result,

$$\begin{aligned} A(\theta) &= [(1 - a)/2ik] \sum_{\ell=0}^L (2\ell + 1) P_{\ell}(\cos \theta) \\ B(\theta) &= 0 \\ d\sigma(\theta)/d\Omega &= [(1 - a)^2/4k^2] \left[\sum_{\ell=0}^L (2\ell + 1) P_{\ell}(\cos \theta) \right]^2 \end{aligned} \quad (8)$$

Physical significance is given to this model by thinking of a spherical interaction region of radius R , where R is the range of the interaction force. Then if the wavelength of the particle being scattered is small compared to R one can think of the scattering as a semi-classical process in which the distance of closest approach of the scattered particle to the center of the scattering force is $\hbar k/p = \ell/k$. Here p is the momentum of the particle and ℓ is the orbital quantum number of a particular angular momentum state. Then for $\ell/k < R$ or $\ell < Rk$ the incoming waves are partially absorbed and $a_\ell < 1$. For $\ell/k > R$ or $\ell > Rk$, there is no interaction and $a_\ell = 1$. With this reasoning Eq. (8) becomes, with $L = Rk$,

$$d\sigma(\theta)/d\Omega = (1 - a)^2 k^2 R^4 \left[J_1(kR\theta)/kR\theta \right]^2, \quad (8a)$$

which is the usual form. This very simple model has only two parameters, R and a , and it does not fit the data at all well.

Our extension of the simple optical model is based on two observations. First, we observed as several authors^{12,13} have, that it is not necessary to use conditions (7). Rather, a more general condition can be used:

$$\delta_\ell^+ = \delta_\ell^- = 0$$

$$a_\ell^+ = a_\ell^- = a_\ell$$

$$a_\ell \approx 0 \text{ (or at least } < 1) \text{ for small } \ell$$

$$a_\ell \rightarrow 1 \text{ as } \ell \rightarrow \infty \quad (9)$$

The physical significance of this generalization is that the idea of an interaction region of range R and uniform strength has been replaced by an interaction region of non-uniform strength. We assume only that the interaction is purely absorptive and that there is zero absorption at very large ℓ values. Remembering that the interpretation is still semi-classical, we associate the a_ℓ at small ℓ values with the strength of the interaction at small distances ℓ/k , the a_ℓ at large ℓ values with the strength of the interaction at large distances ℓ/k . Thus a sudden rise of a_ℓ from nearly 0 to 1 at some ℓ_1 would be interpreted as a sharp drop in the interaction force at distance $r = \ell_1/k$. On the other hand, a slow rise of a_ℓ from 0 to 1 would mean no sharp boundary to the interaction region. Finally, if a_ℓ for small ℓ were larger than a_ℓ for some intermediate ℓ values, this would be interpreted as a hollow core.

A way of visualizing this is to use a graph in which $1 - a_\ell$ is plotted versus ℓ as shown in Fig. 1. Usually the sharp cutoff of the simplest optical model (curve A in Fig. 1) is replaced by a gradual cutoff such as the decline of a Gaussian curve (curve B in Fig. 1). If one assumes that the variation of a_ℓ with ℓ is smooth, then approximate analytic methods can be used to calculate $d\sigma(\theta)/d\Omega$. Two informative papers, one by Greider and Glassgold¹² and the other by Frahn and Venter,¹³ use approximate analytic methods to discuss the generalized optical model, even with $\delta_\ell \neq 0$ and $B(\theta) \neq 0$ in some cases.

Our second observation is that these approximate analytic methods which are very useful for understanding the behavior of $d\sigma(\theta)/d\Omega$ for various assumptions as to a_ℓ behavior, are not appropriate or necessary for $\pi+p$ elastic scattering in the 1 GeV/c to, say, the 10 or 20 GeV/c range. They are not appropriate because in many cases the maximum ℓ value at which a_ℓ is still significantly less than 1, is only 4 or 5, and thus the sum cannot be replaced by an integral. They are not necessary because it is possible to calculate the exact $d\sigma(\theta)/d\Omega$ for any set of a_ℓ values.

But more important, with a computer it is possible to do the reverse problem. Namely, given an experimental differential cross section, one can find the set of real a_ℓ values which gives the best fit to the equation for the differential cross section with purely absorptive scattering

$$d\sigma(\theta)/d\Omega = \left| [1/2ik] \sum_{\ell=0}^L (2\ell + 1)(a_\ell - 1)P_\ell(\cos \theta) \right|^2 . \quad (10)$$

The purely absorptive scattering demands that $0 \leq a_\ell \leq 1$ but with some loss of consistency one may require $-1 \leq a_\ell \leq +1$. This is equivalent to allowing $\delta_\ell \neq 0$, so that $(a_\ell - 1) \rightarrow (a_\ell \cos 2\delta_\ell - 1)$. The loss of consistency comes from not including the $(a_\ell \sin 2\delta_\ell)$ terms.

If there were no constraints on the a_ℓ values then the fitting of the equation

$$[d\sigma(\theta)/d\Omega]^{1/2} = [1/2k] \sum_{\ell=0}^L (2\ell + 1)(a_\ell - 1)P_\ell(\cos \theta) ,$$

which is linear in the parameters a_{ℓ} , can be treated by the standard weighted least squares methods. The constraints on a_{ℓ} make the problem much more difficult and we were fortunate in having available a program written by C. Moore,¹⁴ entitled CURVE, which fits parameters by the standard method of minimizing the weighted sum of the squared residuals.

Given an initial estimate of the parameters a_{ℓ} , the program evaluates the function and obtains the residuals at each of the data points. It is these residuals which are then fitted by using matrix inversion to solve the standard system of normal equations, formed by taking the derivatives with respect to each of the parameters. This procedure yields the correction increments to be applied to the original values of the parameters. In the linear case without constraints, only one iteration is sufficient. However, in the non-linear case, the function having been first expanded by means of a Taylor series, repeated iterations are required, always fitting successive residuals to obtain smaller and smaller correction increments to be applied to the previous set of values of the parameters.

In the case of constraints, the situation becomes slightly unpredictable, since a constraint equation is added to the system if, and only if, the parameter to be constrained falls outside the designated range due to the fact that it was adjusted by too great an amount on the previous iteration. A test on all the constraint cases is made at the end of each iteration, and if a constraint is violated, the appropriate constraint equation is added to the system, and another iteration is required.

III. EMPIRICAL PURELY ABSORPTIVE $\pi^{\pm}+p$ PARTIAL WAVE AMPLITUDES
BELOW 3 GeV/c

In order to make a meaningful application of the least squares method described at the end of the last section, it is necessary to have data on the differential cross section at all angles. Above 3 GeV/c existing $\pi+p$ differential cross-section measurements concern only the diffraction peak; there are no large angle measurements. Therefore, the least squares analysis is only applied to the data at 3 GeV/c and below, which is listed in Table I.

In the fitting of data by an infinite series, the question of how many terms to use always arises. We have used the criterion that the series be extended until the ratio of χ^2/D approaches a minimum and then levels off or rises again. Here χ^2 has the standard meaning of the sum of the squares of the ratios of the residuals to the errors at each data point. D is the degrees of freedom which we have taken as the sum of the number of data points and number of constraints used minus the number of parameters. Table II gives the values of the parameters $(1 - a_{\ell})$ for each set of data for several maximum values of ℓ around this minimum χ^2/D point. The parameters are also given for the kinds of constraints, $0 \leq a_{\ell} \leq 1$, which is designated by I, and $-1 \leq a_{\ell} \leq 1$, which is designated by II. Constraint II, by allowing the additional range $-1 \leq a_{\ell} < 0$, implies that $\pi \geq |\delta_{\ell}| \geq \pi/2$ is being allowed, or that at least $2\delta_{\ell} = \pi$ is being allowed. Thus Constraint II allows at least a 90° phase shift in addition to the 0° phase shift of Constraint I.

We first observe that the II constraint always gives better fits, and sometimes substantially better fits, than the I constraint. However, we also observe that it is only a_0 which requires the II constraint. That is, it is only the S wave which is not purely absorptive. There is no particular reason known for the S wave to be exempt from the I constraint, but it is probable that the improvement in the fit when $1 - a_0 > 1$ is due to the S wave taking up some of the neglected non-absorptive and spin-flip scattering.

We have taken the II constraint parameters as being most meaningful and Figs. 2 and 3 show the kinds of fits which are achieved. To simplify the comparisons, experimental cross sections at each momenta are divided by the quantity $(k\sigma_{\text{tot}}/4\pi)^2$. This is the 0° differential cross section given by the optical theorem if the scattering amplitude has no real part. Since the real part is small, this normalized $d\sigma/d\Omega$ goes roughly to 1.0 at 0° . The fitted curves follow the data quite well and in no case is there a deviation between the two which could not be taken account of by a small amount of non-absorptive or spin-flip scattering. These neglected scattering terms could also account for the low χ^2 probabilities which are listed in Table II. However, these χ^2 probabilities should not be taken too seriously because the errors used were purely statistical. No account was taken of systematic errors in the instrument or the analysis. In many of the experiments it is reasonable to take the systematic errors as very roughly equal to the statistical errors, which immediately increases the probabilities drastically. These χ^2 probabilities are also listed in Table II.

A few comments on Figs. 2 and 3 will now be made. All the plots are semilogarithmic so that the fluctuations of the cross section at larger angles (where statistics are poorer) are exaggerated. Similarly, the deviations of the fitted curves from the data at these larger angles seem to be more important than they really are. Conversely, the diffraction peak has a very strong effect on the a_ℓ values because of the relatively high statistics of the points on the peak.

For π^-+p at 1.33 GeV/c the fit at large angles is poor; since this momentum is relatively low, the purely absorptive assumption may be quite poor here. However, some of the fluctuations in the data occur over such a small region of $\cos \theta$, that there is some possibility that there are errors in the data, or that higher ℓ values are needed. For π^++p at 1.33 GeV/c the purely absorptive assumption is definitely wrong. The reason for the fitted curve lying almost always below the data is that $1 - a_0 \leq 2$ was required. A further increase in $1 - a_0$ immediately improves the fit. This 1.33 π^++p data of Helland⁷ has been fit by him with an equation of the form

$$\sum_{i=0}^7 C_i (\cos \theta)^i$$

with no constraints on the C_i . He obtains a good fit but this series cannot be resolved uniquely into our a_ℓ and δ_ℓ values, so we cannot interpret it. To see if small amounts of higher ℓ states would improve these low momenta fits we have tried higher order fits which are the dashed curves in Figs. 2a and 3a. The π^-+p curve for these higher orders fits the data well, but the π^++p fit remains poor. This may be related to the resonance in the π^++p total cross section at this momentum.

Whether the fitted $d\sigma/d\Omega$ turns up or down as θ approaches 180° depends on the data near that point. In general, we find either large uncertainties or possibly unrealistic fluctuation in $d\sigma/d\Omega$ near 180° . Thus the $d\sigma/d\Omega$ in 1.50 GeV/c π^+p at 180° very probably turns up the way it does at 1.55 GeV/c π^+p ; however, the statistics of the last point at 1.50 GeV/c are not sufficiently high to force the turn up, unless l_{\max} is increased. The backward peak in the 2.92 GeV/c π^+p and 3.15 GeV/c π^-p data comes from the fit at smaller angles and there is no proof of its existence.

Finally, in the 2.02 GeV/c π^+p we have also tried higher l_{\max} fits (the dotted and dashed curves) although the statistics do not warrant doing this. The dotted curve which has $l_{\max} = 10$ turns up at 180° while the dashed curve which has $l_{\max} = 9$ turns down, although both of these curves follow the data quite well. Once again this indicates the uncertainties at 180° in $d\sigma/d\Omega$.

Of course, there is no proof that the parameters of Table II are unique. It is certainly possible by using large amounts of non-absorptive and spin-flip scattering to get drastically different answers. However, on the assumption that the scattering is mainly absorptive, the parameters of Table II provide a set of partial wave amplitudes which describe quite well all the varied shapes of the existing data. To visualize how these partial wave amplitudes vary with l , $1 - a_l$ is plotted versus l for π^+p in Fig 4 and π^-p in Fig. 5.

IV. EMPIRICAL PARTIAL WAVE AMPLITUDES ABOVE 3 GeV/c

To fit the data above 3.15 GeV/c we have extended a method of Minami¹⁶ in which the data is first expressed in the form

$$d\sigma/d\Omega = [A(\theta)]^2$$

$$A(\theta) = \exp(a_0 + a_1 \cos \theta) + c + \exp(-b_0 - b_1 \cos \theta).$$

This is a form suggested by the simple Regge theory in which the first term is the exponential diffraction peak, the last term is a possible peak for 180° scattering and c is a constant background term. Minami uses this form to show the effect of the possible, but so far undetected, backward peak on the partial wave amplitudes. For this simple form the partial wave amplitudes can be found analytically. For $\pi^- + p$ at 4.13 GeV/c, Minami gives a_ℓ for the case in which there is no backward peak and for the case in which the backward peak is $1/24$ of the diffraction peak in height. His values in the form $1 - a_\ell$ are given in Table III. The major difference between the $1 - a_\ell$ values in the two cases is that if there is no backward peak, $1 - a_\ell$ decreases monotonically, whereas if there is a backward peak, $1 - a_\ell$ oscillates for small ℓ . This is a phenomenon which we frequently observed in the course of these fits at momenta above 2 GeV/c. The diffraction peak can be fit by a monotonically decreasing series of $1 - a_\ell$ values or by a series in which either the even ℓ or odd ℓ values of $1 - a_\ell$ are larger. However, the second situation always leads to a backward peak. This can be understood by realizing that for θ close to 0, all $P_\ell(\cos \theta)$ are positive and the partial waves

add. For θ close to 180° , the $P_\ell(\cos \theta)$ are positive for even ℓ and negative for odd ℓ . If the amplitudes are monotonically decreasing, then there will be almost complete cancellation at 180° . But, if the even ℓ or odd ℓ amplitudes are unusually larger, there will be a residual backward peak.

For 4.95 GeV/c, π^-+p we have used the exponential fit of Perl et al.¹⁰

$$d\sigma/d\Omega = \exp(3.64 + 8.9t + 2.0t^2 + 0.1t^3),$$

where t is the square of the four momentum transfer in $[\text{GeV}/c]^2$.

The expansion in partial waves,

$$\left[\exp(3.64 + 8.9t + 2.0t^2 + 0.1t^3) \right]^{\frac{1}{2}} = [1/2k] \sum_{\ell=0}^L (1 - a_\ell)(2\ell + 1)P_\ell(\cos \theta),$$

was carried out by numerical integration. The $1 - a_\ell$ values are listed in Table IV.

Figure 6 shows the $1 - a_\ell$ versus ℓ plots for the no backward peak case for 4.13 GeV/c and for 4.95 GeV/c. The $1 - a_\ell$ versus ℓ behavior is a clear continuation of the behavior at lower energies.

For the very high momenta such as the measurement of Caldwell et al.,⁵ or of Foley et al.,⁴ there is no point in writing down all the partial wave amplitudes at this time since the large angle differential cross section is completely unknown. At higher energies the $\pi^\pm+p$ differential cross section has very close to an exponential shape in t . Therefore, the $1 - a_\ell$ versus ℓ behavior as exhibited at lower energies will continue, namely, there will be a $1 - a_\ell$ versus ℓ behavior such as in Fig. 6, with $1 - a_0 < 1$ and a slow decrease in $1 - a_\ell$ as ℓ increases. It is interesting to observe that below

3.15 GeV/c the best fit requires $1 - a_0 > 1$, but that above 3.15 GeV/c all $1 - a_\ell$ are less than 1, so that above 3.15 GeV/c the fit can be purely absorptive.

V. COMPARISON WITH OTHER MODELS

The fits to the data found in Section III are much superior to the fits obtained using the standard optical models. To illustrate this, we have made the best fits to the data using the following models for a_ℓ :

Sharp Cutoff Rectangular Model:

$$1 - a_\ell = 1 - a, \quad 0 \leq \ell \leq \ell_{\max}$$

$$1 - a_\ell = 0, \quad \ell > \ell_{\max}$$

Sharp Cutoff Gaussian Model:

$$1 - a_\ell = 3/\ell_{\max} \sqrt{2\pi}, \quad 0 \leq \ell \leq \ell_{\max}$$

$$1 - a_\ell = (3/\ell_{\max} \sqrt{2\pi}) \exp(-9(\ell - \ell_{\max})^2/2\ell_{\max}^2), \quad \ell > \ell_{\max}$$

Median Cutoff Gaussian Model:

$$1 - a_\ell = 3/2\ell_{\max} \sqrt{2\pi}, \quad 0 \leq \ell \leq \ell_{\max}$$

$$1 - a_\ell = (3/2\ell_{\max} \sqrt{2\pi}) \exp(-9(\ell - \ell_{\max})^2/8\ell_{\max}^2), \quad \ell > \ell_{\max}$$

Pure Gaussian Model:

$$1 - a_\ell = (1/\ell_{\max} \sqrt{2\pi}) \exp(-\ell^2/2\ell_{\max}^2), \quad \text{all } \ell$$

The sharp cutoff rectangular model is self-explanatory: the coefficients are constant up to some maximum value of ℓ , after which the $1 - a_\ell$ are zero. In the sharp and medium Gaussian cutoff models,

we have held the parameters constant up to some maximum ℓ , and then let them decrease by following a Gaussian curve in which the mean is ℓ_{\max} , and the variance is $\ell_{\max}/3$ and $2\ell_{\max}/3$, respectively. The pure Gaussian model represents an immediate Gaussian decrease in the values of the $1 - a_{\ell}$, with no constant sequence at the beginning; that is, the mean is equal to ℓ_{\max} , which is equal to zero.

Figure 7 shows the fit for the Sharp Cutoff Rectangular Model (A), the fit for the best of the Gaussian Models (B), and the fit of Section III (C), for $2.01 \pi^{-}p$ and $3.15 \pi^{-}p$. In considering the goodness of fit of the models, one can neglect the points at which the calculated curves go to 0. These points look very bad because semi-logarithmic plots are being used, but a small amount of non-absorptive or spin-flip scattering can adjust these points. However, the important observations are first, that the Gaussian models are no improvement over the Rectangular Model in spite of the usually held idea that a Gaussian Model is more realistic. Secondly, both models deviate from the data at both large angles, and in the diffraction peak. Finally, they clearly need major modification (such as adding a constant term) to improve the fit, so that one might as well go directly to the fits of Section III.

VI. DISCUSSION OF THE PURELY ABSORPTIVE WAVE AMPLITUDES

The conclusion from the last three sections is that we have found a set of a_ℓ values which change in a smooth way with energy and which fit the data quite well. Except for the S-wave all the $1 - a_\ell$ are less than one. The maximum ℓ used is roughly 1.5 to 2 times kR if R is taken as 10^{-13} cm. All of this is in accord with some optical models which have been previously used. However, there is a very important difference between all previous models and these sets of parameters. In previous models the values of $1 - a_\ell$ are taken as 1 up to some ℓ' , and then $1 - a_\ell$ drops to 0 quickly or slowly depending on how sharp a cutoff is assumed.

However, looking at Figs. 4 and 5, it can be observed that, for all our sets of parameters, $1 - a_\ell$ decreases continuously to 0 with no indication of a break or change in the shape of $1 - a_\ell$ versus ℓ . There is no evidence of a surface region. The shape of the $1 - a_\ell$ versus ℓ curve lies between linear and concave upward, and no inelastic channel is completely absorbed except for the S channel. In terms of the pion-nucleon interaction this means that the rough picture is one in which the forces decrease smoothly with distance, and which indicates no surface region in which the forces change rapidly.

Of course this is the picture given by field theory also, and the diffuseness of the pion-nucleon interaction is, therefore, no surprise. Perhaps the main point of this analysis is not the behavior of the large ℓ value amplitudes, which have always been assumed to be decreasing smoothly to 0. The point is that even the low ℓ states, such as p and d , are incompletely absorbed.

We now turn to the relation between these a_ℓ fits and the higher pion-nucleon resonances. As discussed in the Introduction, Simmons⁹ has shown that the Sharp Cutoff Rectangular Model can explain the second peak at 2.0 GeV/c in the $\pi^\pm + p$ differential cross section. Reference to Table II shows that the fitted values of $1 - a_\ell$, which reproduce the data quite well, exhibit no particularly large $1 - a_\ell$ value; that is, no ℓ state seems to predominate. Therefore, we agree with Simmons that the $\pi^\pm + p$ differential cross sections give no evidence as to the angular momentum states which cause the 2.1 GeV/c maximum in the $\pi^\pm + p$ total cross section.

Furthermore, the several fits to the $\pi^+ + p$ data in the 1.5 GeV/c region show no dominant high angular momentum state. Therefore, the large backward bump in the differential cross sections at these momenta may not be related at all to the $\pi^+ + p$ total cross-section maxima at 1.4 GeV/c. As has been stated before, these fits may not be unique and there may be a set of amplitudes, particularly when non-absorptive and spin-flip scattering appear, which do show that a higher ℓ state is particularly large.

In connection with this, it is important to know that the sizes of the coefficients c_n in an expansion of the form

$$d\sigma(\theta)/d\Omega = \sum_{n=0}^N c_n [\cos \theta]^n \quad (11)$$

are not directly indicative of the importance of a particular ℓ state. For example, if one considers a Sharp Cutoff Rectangular Model of the

form

$$1 - a_{\ell} = 1, \quad 0 \leq \ell \leq 3$$

$$1 - a_{\ell} = 0, \quad \ell > 3.$$

then the relative sizes of the coefficients when $d\sigma/d\Omega$ is expressed in the form of Eq. (11) are

$$c_0 = 1$$

$$c_1 = 9.1$$

$$c_2 = 15.4$$

$$c_3 = -52.4$$

$$c_4 = -91.2$$

$$c_5 = 115.7$$

$$c_6 = 136.1$$

Thus, one might be tempted to ascribe particular importance to $\ell = 2$ or $\ell = 3$ states since the c_4 , c_5 , and c_6 coefficients are so large, whereas all states actually enter with exactly equal absorption.

As another example, consider a model with

$$1 - a_0 = 1$$

$$1 - a_1 = 1/3$$

$$1 - a_2 = 1/5$$

$$1 - a_3 = 1/7$$

$$1 - a_4 = 1/9$$

$$1 - a_5 = 1/11$$

$$1 - a_6 = 1/13$$

$$1 - a_{\ell} = 0, \quad \ell > 6.$$

The relative c_n coefficients are:

$$\begin{aligned}c_0 &= +1.0 \\c_1 &= +0.8 \\c_2 &= -2.8 \\c_3 &= -4.6 \\c_4 &= -8.4 \\c_5 &= -0.0 \\c_6 &= -5.0 \\c_7 &= +41.5 \\c_8 &= +43.9 \\c_9 &= -71.4 \\c_{10} &= -64.0 \\c_{11} &= +38.5 \\c_{12} &= +35.0\end{aligned}$$

Here again, the higher ℓ states seem to predominate, whereas there is actually a smooth dropoff in the absorption as ℓ increases.

VII. INCLUSION OF NON-ABSORPTIVE AND SPIN-FLIP SCATTERING

Our original hope of being able to make complete fits using the full Eq. (6a) was not fulfilled for two reasons. First, the computer problem proved to be very difficult since Eq. (6a) is non-linear and there are constraints on a_ℓ^\pm and δ_ℓ^\pm . Unless the program was given initial values for the parameters quite close to the best fit parameters, the computation converged either very slowly or not at all.

Frequently, as the iteration proceeded, some constraints went in and out of the calculation repeatedly so that the iteration became cyclic. Therefore, in many cases when we attempted a complete fit we found no solution and in no case could we be sure that we had found the solution with the lowest χ^2 .

The second reason is that much more extensive data is required. Not only is there the obvious need for polarization data to give the spin-flip scattering, but for the differential cross section both good statistics and close data spacing are required. For example, we find at 2.01 GeV/c π^-+p that the exact shape of the diffraction peak strongly controls the values of a_ℓ . This is the reason that the fit to the second peak is not exact. Also, even though there are 7000 events in this measurement, the statistics at large angles are insufficient. On the other hand, in the 1.55 GeV/c π^++p data there are good statistics at large angles, but the diffraction peak was not measured at small enough angles, so its slope is relatively unsure, and the values of a_ℓ may be somewhat inaccurate.

However, as a first look at more complete fitting, we have taken the 2.01 GeV/c π^-+p data of Damouth et al.⁸ This data, which has only been published previously in graphical form, is given in the Appendix along with the 2.02 GeV/c π^++p data of Damouth et al.⁸

The differential cross section is written in the form

$$d\sigma(\theta)/d\Omega = [1/4k^2] \left\{ \left[\sum_{\ell=0}^{\ell_{\max}} (2\ell + 1)(1 - a_\ell) P_\ell(\cos \theta) \right]^2 + \sum_{i=0}^{i_{\max}} b_i (\cos \theta)^i \right\} \quad (12)$$

The b_i series is designed to allow for spin-flip scattering and the $\sin 2\delta_l$ part of the non-absorptive scattering. The a_l were constrained so that $0 \leq 1 - a_l \leq 2$ and the b_i were constrained so that

$$\sum_{i=0}^{i_{\max}} b_i (\cos \theta)^i \geq 0, \quad \text{for all } \theta. \quad (13)$$

Figure 8 indicates the improved fit to the data, given by the solution in Table V. Table VI lists $d\sigma(\theta)/d\Omega$ and the contribution of the b_i series for a selection of $\cos \theta$ values. In the very small angle region the b_i contribution is always less than 10%, which agrees with the requirement that the real part of the scattering amplitude and the spin-flip scattering amplitude be small in this region. For some of the large angles, however, the b_i contribution is the major part, but here there are as yet no theoretical ideas with which to compare these predictions.

APPENDIX

Pion-proton differential cross section in barycentric system.
 The errors are statistical and do not include an overall normalization error of $\pm 8\%$ for π^-+p and $+10\%$, -20% for π^++p .

π^-+p scattering at 2.01 GeV/c

<u>cos θ</u>	<u>dσ/dΩ (mb/sr)</u>
.935	6.04 \pm .28
.925	5.28 \pm .27
.915	4.74 \pm .25
.905	3.92 \pm .24
.890	3.16 \pm .15
.870	2.54 \pm .14
.850	2.13 \pm .13
.83	1.86 \pm .12
.81	1.45 \pm .11
.79	1.02 \pm .09
.77	.79 \pm .08
.75	.63 \pm .07
.73	.54 \pm .07
.71	.35 \pm .06
.69	.25 \pm .05
.66	.20 \pm .03
.62	.14 \pm .03
.58	.06 \pm .02
.54	.10 \pm .02
.50	.05 \pm .02

Appendix (cont'd)

 π^-+p scattering at 2.01 GeV/c

<u>cos θ</u>	<u>$d\sigma/d\Omega$ (mb/sr)</u>
.46	.08 \pm .02
.42	.11 \pm .03
.38	.17 \pm .03
.34	.15 \pm .03
.30	.18 \pm .03
.26	.23 \pm .03
.22	.25 \pm .04
.18	.18 \pm .03
.14	.23 \pm .03
.10	.14 \pm .03
.06	.16 \pm .03
.02	.11 \pm .02
-.02	.16 \pm .03
-.06	.14 \pm .03
-.10	.09 \pm .02
-.16	.08 \pm .01
-.24	.06 \pm .01
-.32	.06 \pm .01
-.40	.05 \pm .01
-.48	.06 \pm .01
-.56	.04 \pm .01
-.64	.02 \pm .01
-.72	.01 \pm .01
-.80	.01 \pm .01
-.88	.02 \pm .01
-.94	.03 \pm .02

Appendix (cont'd)

 π^+p scattering at 2.01 GeV/c

<u>cos θ</u>	<u>$d\sigma/d\Omega$ (mb/sr)</u>
.93	6.54 \pm .74
.91	4.89 \pm .64
.89	3.42 \pm .38
.86	3.35 \pm .27
.82	2.35 \pm .23
.775	1.56 \pm .17
.725	1.06 \pm .14
.650	.43 \pm .07
.55	.29 \pm .05
.45	.18 \pm .04
.35	.25 \pm .05
.25	.26 \pm .05
.15	.32 \pm .05
.05	.09 \pm .03
-.05	.13 \pm .04
-.15	.14 \pm .04
-.25	.12 \pm .04
-.35	.18 \pm .04
-.45	.07 \pm .03
-.55	.12 \pm .04
-.65	.09 \pm .04
-.75	.03 \pm .03
-.85	.04 \pm .03
-.93	.06 \pm .05

ACKNOWLEDGEMENT

We wish to thank C. Moore for the use of his curve fitting program which made this work easier. We also wish to thank P. Carruthers, L. M. Simmons, and S. Minami for their letters and preprints which gave us considerable insight.

LIST OF REFERENCES

1. Table I and references 4, 5, 10, 15.
2. S.C. Frautschi, M. Gell-Mann and F. Zachariasen, Phys. Rev. 126, 2204 (1962).
3. S.D. Drell in Proceedings of the 1962 International Conference on High Energy Physics at CERN (CERN, Geneva, 1962); p. 897.
4. K.J. Foley, S.J. Lindenbaum, W.A. Love, S. Ozaki, J.J. Russell, and L.C.L. Yuan, Phys. Rev. Letters 10, 376 (1963).
5. D.O. Caldwell, B. Elsnor, D. Harting et al., Physics Letters 8, 288 (1964).
6. V. Cook, B. Cork, W.R. Holly, and M. L. Perl, Phys. Rev. 130, 762 (1963).
7. J.A. Helland, University of California Radiation Laboratory Report No. UCRL-10378 (1962).
8. D.E. Damouth, L.W. Jones, and M.L. Perl, Phys. Rev. Letters 11, 287 (1963).
9. L.M. Simmons, Phys. Rev. Letters 12, 229 (1964).
10. M.L. Perl, L.W. Jones, and C.C. Ting, Phys. Rev. 132, 1252 (1963).
11. L. Schiff, Quantum Mechanics (McGraw-Hill, New York, 1949); p. 103.
12. K.R. Greider and A.E. Glassgold, Ann. Phys. (N.Y.) 10, 100 (1960).
13. W.E. Frahn and R.H. Venter, Ann. Phys. (N.Y.) 24, 243 (1963).
14. C. Moore, private communication.
15. S. Brandt, V.T. Cocconi, D.R.O. Morrison et al., Phys. Rev. Letters 10, 413 (1963).
16. S. Minami, Phys. Rev. 133, B1581 (1964).

FIGURE CAPTIONS

1. Two possible models for the dependence of $1 - a_\ell$ on ℓ . Curve A is the Sharp Cutoff Rectangular Model and curve B is the Medium Cutoff Gaussian Model, both defined in Section V.
2. Data and fitted curves for π^+p systems. $d\sigma/d\Omega$ is normalized by dividing the experimental differential cross section by $(k\sigma_{\text{tot}}/4\pi)^2$. The vertical bars indicate the statistical experimental errors. The meaning of the solid and dashed curves is given in Table II and in the text.
3. Data and fitted curves for π^-p systems. $d\sigma/d\Omega$ is normalized by dividing the experimental differential cross section by $(k\sigma_{\text{tot}}/4\pi)^2$. The vertical bars indicate the statistical experimental errors. The meaning of the solid and dashed curves is given in Table II and in the text.
4. Values of $1 - a_\ell$ for π^+p systems. The vertical bars indicate the statistical errors in the coefficients. These coefficients apply only to the solid curves of Fig. 2.
5. Values of $1 - a_\ell$ for π^-p systems. The vertical bars indicate the statistical errors in the coefficients. These coefficients apply only to the solid curves of Fig. 3.
6. Values of $1 - a_\ell$ for π^-p systems at 4.13 GeV/c and 4.95 GeV/c.
7. Data and fitted curves for the Sharp Cutoff Rectangular Model (A), the best of the Gaussian Models (B), and the fit of Section III, for π^-p systems at 2.01 and 3.15 GeV/c.
8. Data and plot of curve for 2.01 GeV/c π^-p system, fitted with inclusion of terms for non-absorptive and spin-flip scattering.

TABLE I

List of experimental differential cross sections below
and at 3.15 GeV/c which are analyzed in Section III.

<u>System</u>	<u>Initial Laboratory Momentum in GeV/c</u>	<u>Reference</u>
$\pi^- + p$	1.33	a
$\pi^+ + p$	1.33	b
$\pi^- + p$	1.50	c,d
$\pi^+ + p$	1.50	e
$\pi^+ + p$	1.55	b
$\pi^- + p$	1.59	f
$\pi^+ + p$	2.00	e
$\pi^- + p$	2.01	g
$\pi^+ + p$	2.02	g
$\pi^+ + p$	2.50	e
$\pi^+ + p$	2.92	h
$\pi^- + p$	3.15	h

FOOTNOTES TO TABLE I

- a. L. Bertanza, R. Carrara, A. Drago, P. Franzini, I. Mannelli, G.V. Silvestrini, and P.H. Stoker, *Nuovo Cimento* 19, 467 (1961).
- b. J. Helland, University of California Radiation Laboratory Report UCRL-9507, (1962).
- c. M. Chretien, J. Leitner, N.P. Sanios, M. Schwartz, and J. Steinberger, *Phys. Rev.* 108, 383 (1957).
- d. K.W. Lai, L.W. Jones, and M.L. Perl, *Phys. Rev. Letters* 7, 125 (1961).
- e. V. Cook, B. Cork, W. Holly, and M.L. Perl, *Phys. Rev.* 130, 762 (1963).
- f. J. Alitti, J.P. Barton, A. Berthelot, *Nuovo Cimento* 29, 515 (1963).
- g. D. E. Damouth, L.W. Jones, and M. L. Perl, *Phys. Rev. Letters* 11, 287 (1963).
- h. M.L. Perl, L.W. Jones, and C.C. Ting, *Phys. Rev.* 132, 1252 (1963).

TABLE II (Page 4 of 4)

System	π^-+p	π^-+p	π^-+p
Incident Lab Momentum (GeV/c)	2.00	3.15	3.15
Plot	solid curve	solid curve	none
Constraint Type	II	II	II
Max ℓ	6	8	9
D	39	15	14
χ^2	103.69	36.42	34.42
$P(\chi^2)$	< .005	< .005	< .005
$P(\chi^2/2)$.10	.25	.25
1-a ₀	1.365 ± .013	1.09 ± .04	1.06 ± .04
1-a ₁	0.6344 ± .0084	0.688 ± .022	0.718 ± .031
1-a ₂	0.3581 ± .0076	0.515 ± .022	0.497 ± .025
1-a ₃	0.2739 ± .0062	0.352 ± .017	0.383 ± .028
1-a ₄	0.2094 ± .0060	0.289 ± .019	0.272 ± .022
1-a ₅	0.0935 ± .0048	0.171 ± .014	0.196 ± .022
1-a ₆	0.0279 ± .0047	0.116 ± .013	0.102 ± .016
1-a ₇		0.050 ± .011	0.064 ± .015
1-a ₈		0.036 ± .012	0.029 ± .013
1-a ₉			0.017 ± .012
1-a ₁₀			
1-a ₁₁			

TABLE III

 $1 - a_\ell$ values for $\pi^- + p$ at 4.13 GeV/c, given by Minami.¹⁶

ℓ	$1 - a_\ell$	
	No Backward Peak	Backward Peak
0	1.00	0.76
1	0.73	0.95
2	0.61	0.44
3	0.50	0.62
4	0.48	0.31
5	0.27	0.30
6	0.18	0.16
7	0.11	0.12
8	0.06	0.06
9	0.03	0.04
10	0.02	0.02
11	0.01	0.01
12	0.004	0.004

TABLE IV

1 - a_ℓ values for $\pi^- + p$ at 4.95 GeV/c.

ℓ	$1 - a_\ell$
0	0.89
1	0.82
2	0.69
3	0.57
4	0.46
5	0.35
6	0.24
7	0.18
8	0.13
9	0.09
10	0.07
11	0.05

TABLE V

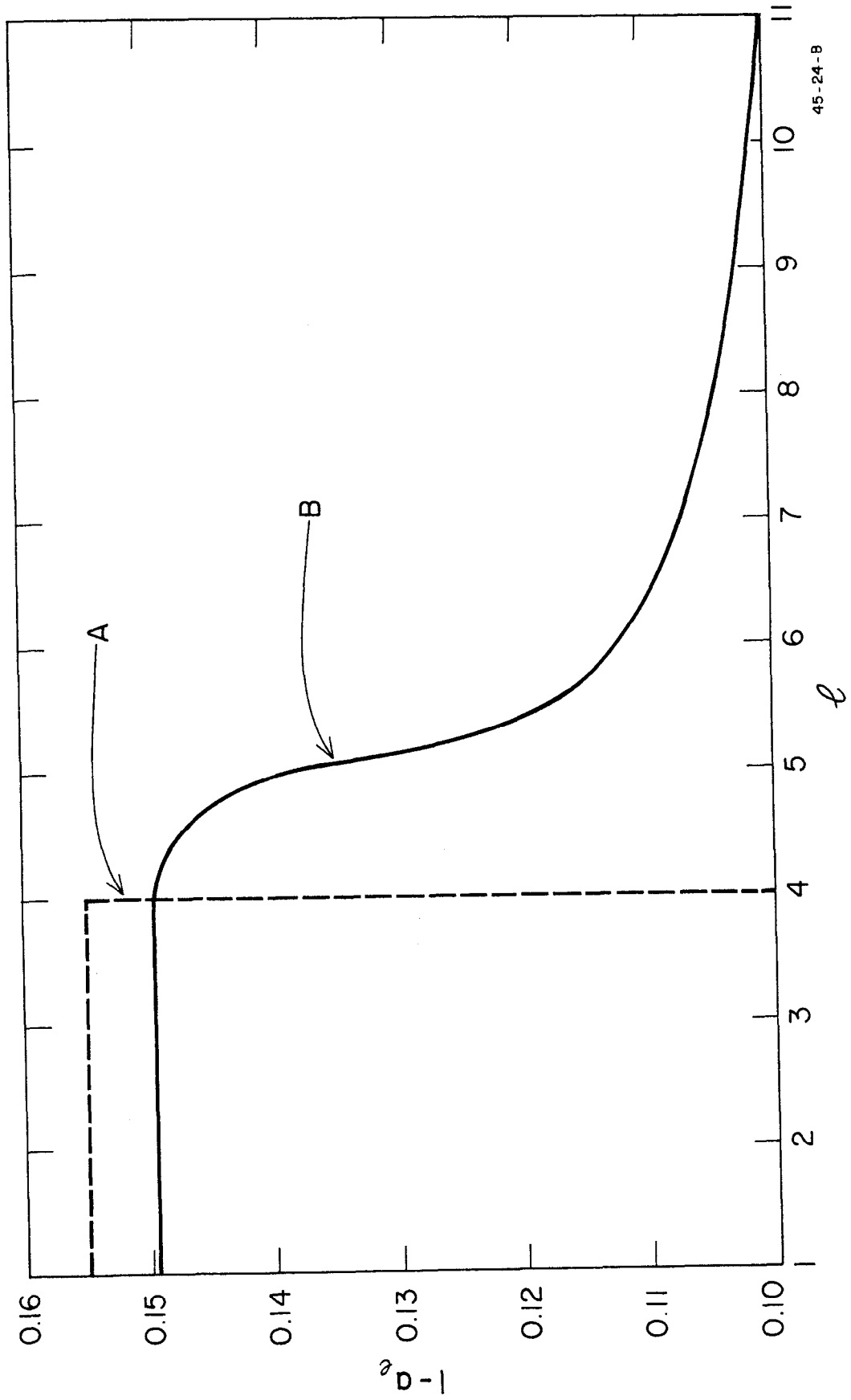
 $1 - a_\ell$ values and b_i values for π^-+p at 2.01 GeV/c

<u>ℓ</u>	<u>$1 - a_\ell$</u>	<u>i</u>	<u>b_i</u>
0	0.99	0	0.50566
1	0.689	1	-0.29936
2	0.383	2	-3.12056
3	0.172	3	-0.5424
4	0.226	4	5.8152
5	0.117	5	4.11546

TABLE VI

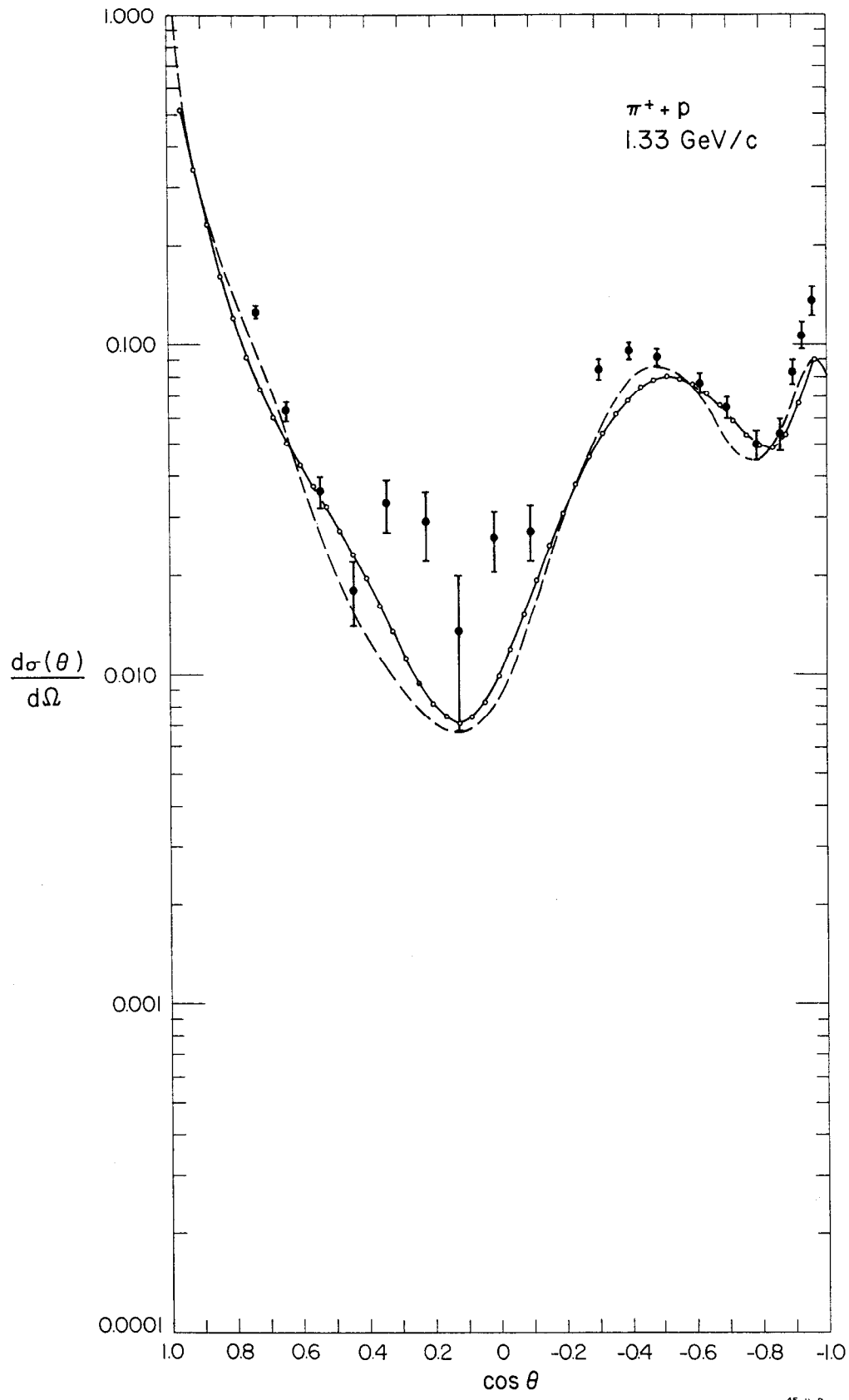
Fitted values of Eq. (12) given by solution in Table V for π^-+p data at 2.01 GeV/c. Both terms have been normalized to show relative size of b_i term.

$\cos \theta$	$d\sigma/d\Omega$	$\sum_{i=0}^5 b_i (\cos \theta)^i$
0.935	0.36740	0.03565
0.850	0.12990	0.02025
0.750	0.03650	0.00894
0.620	0.00822	0.00183
0.540	0.00499	0.00026
0.460	0.00538	0.00000
0.380	0.00754	0.00052
0.300	0.01014	0.00014
0.220	0.01194	0.00240
0.140	0.01220	0.00324
0.060	0.01085	0.00383
-0.020	0.00847	0.00410
-0.100	0.00595	0.00406
-0.240	0.01268	0.00339
-0.400	0.00335	0.00215
-0.560	0.00257	0.00109
-0.720	0.00064	0.00058
-0.880	0.00139	0.00030



45-24-B

FIG. 1



45-11-0

FIG. 2a

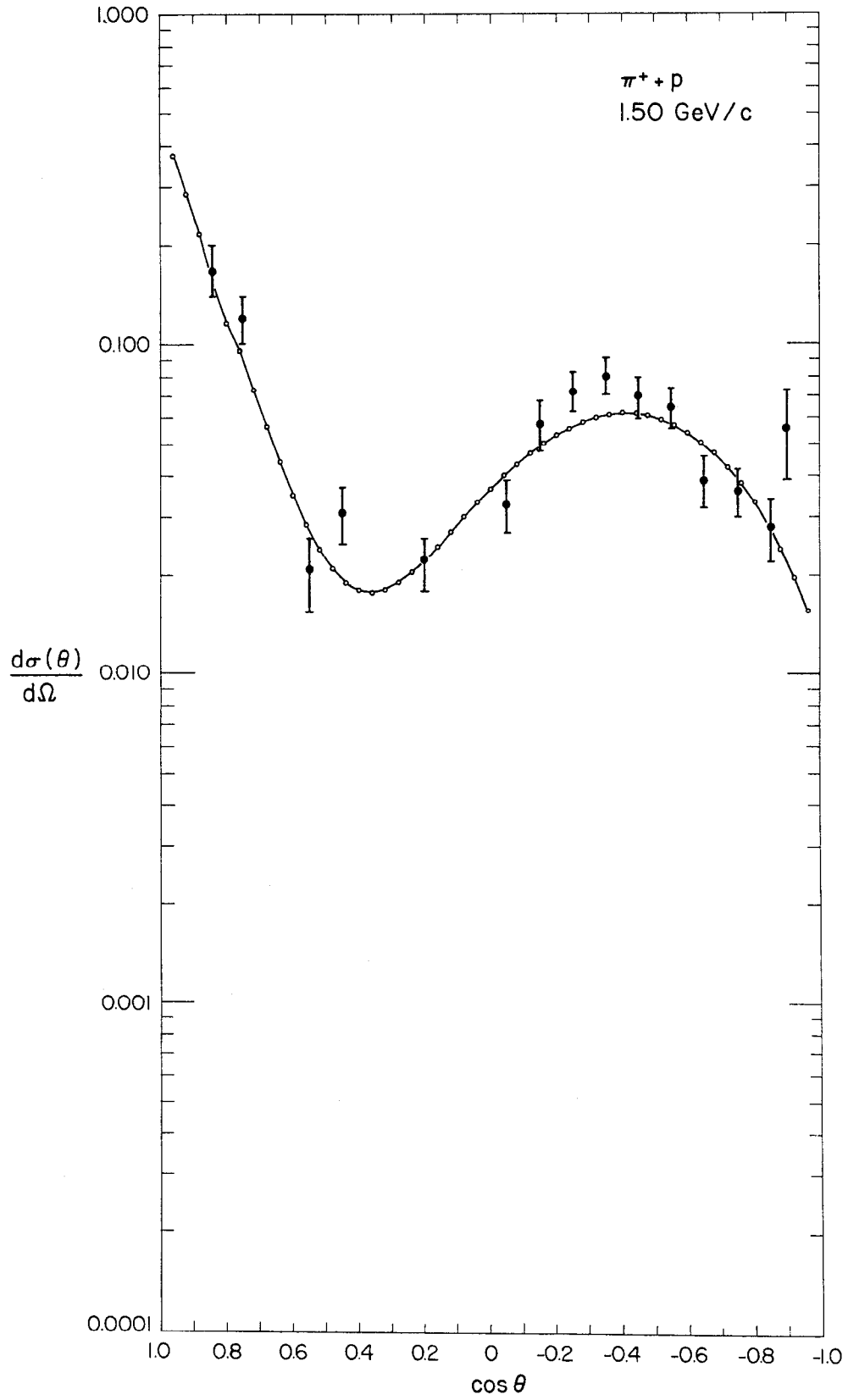


FIG. 2b

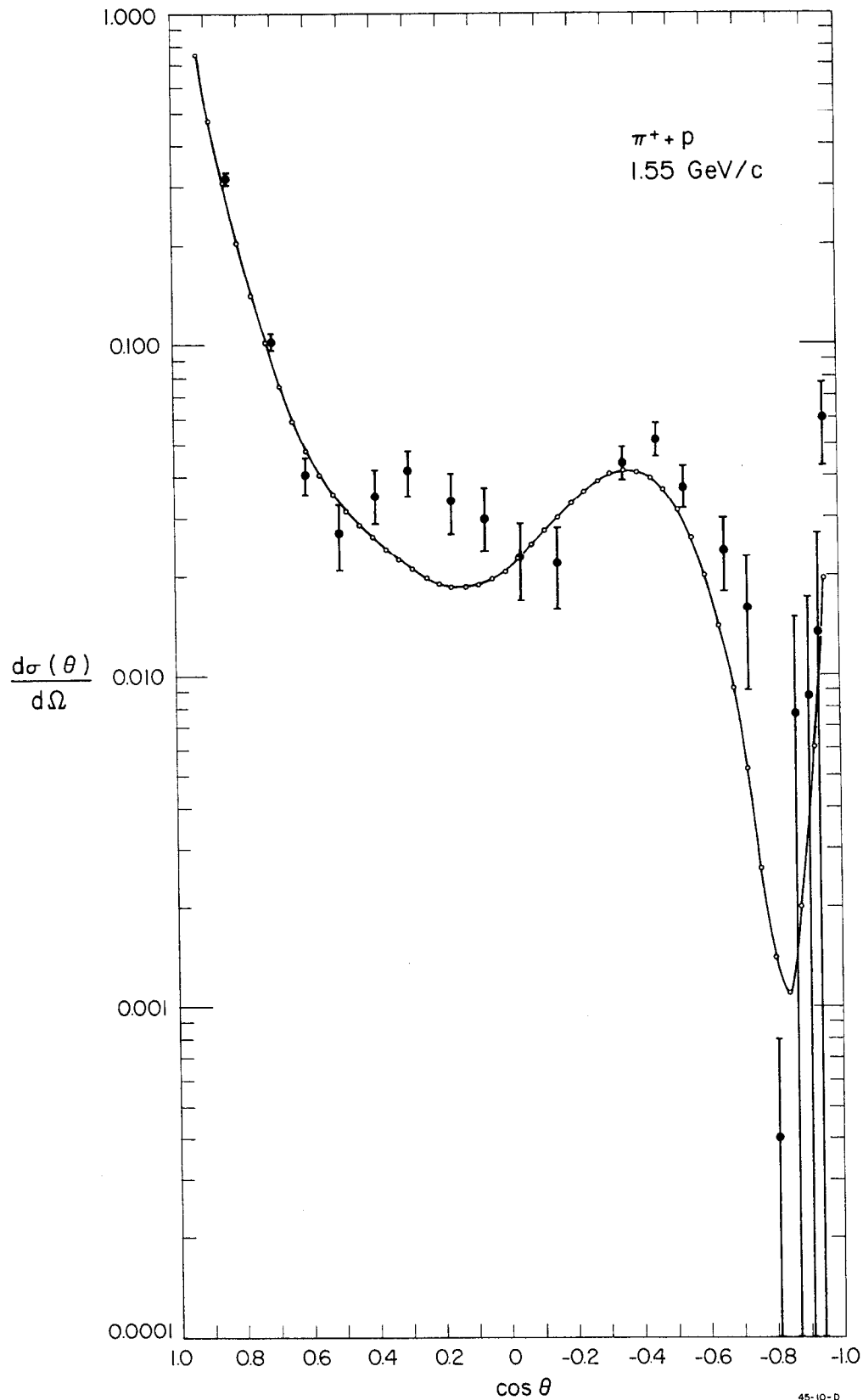


FIG. 2c

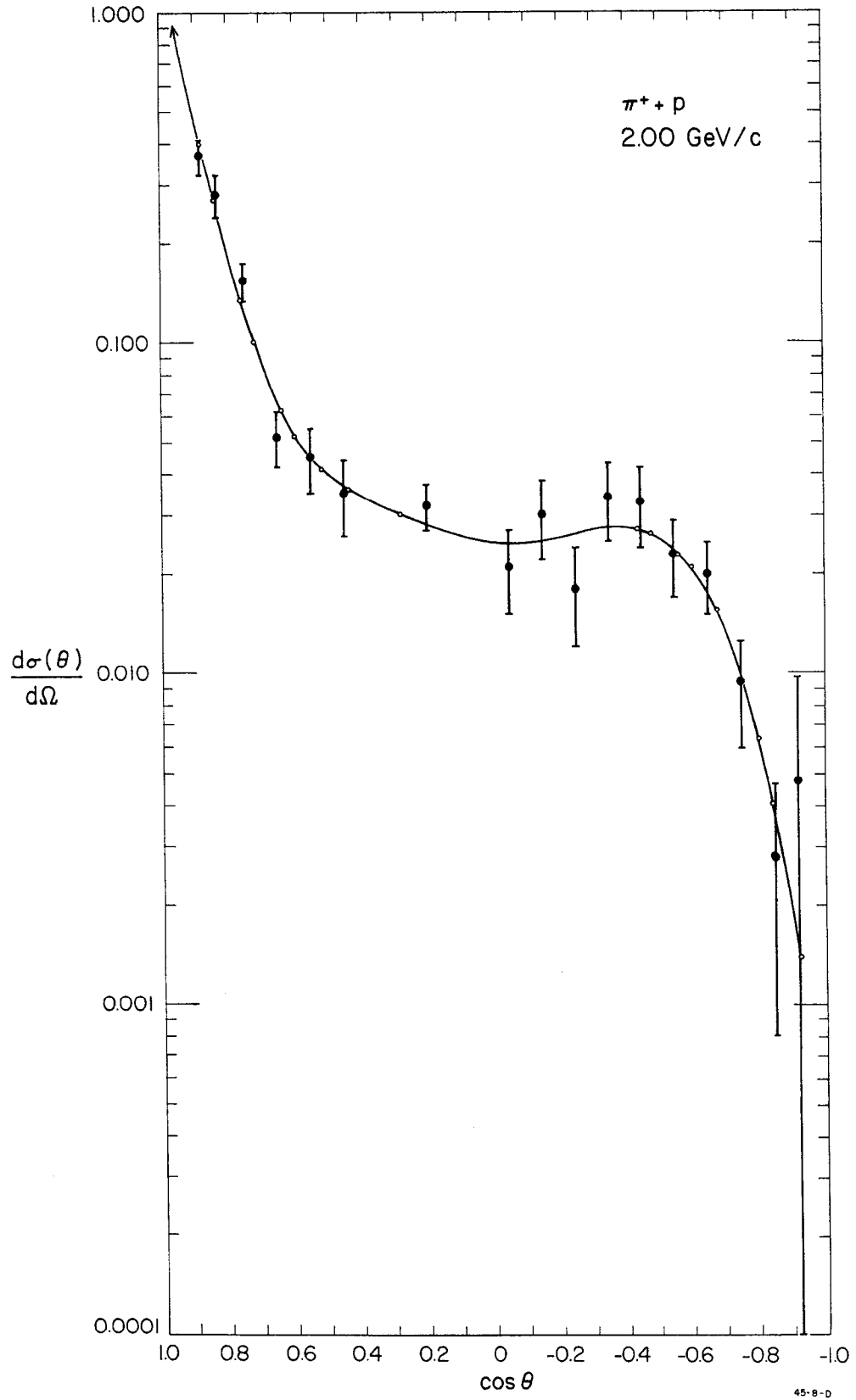


FIG. 2d

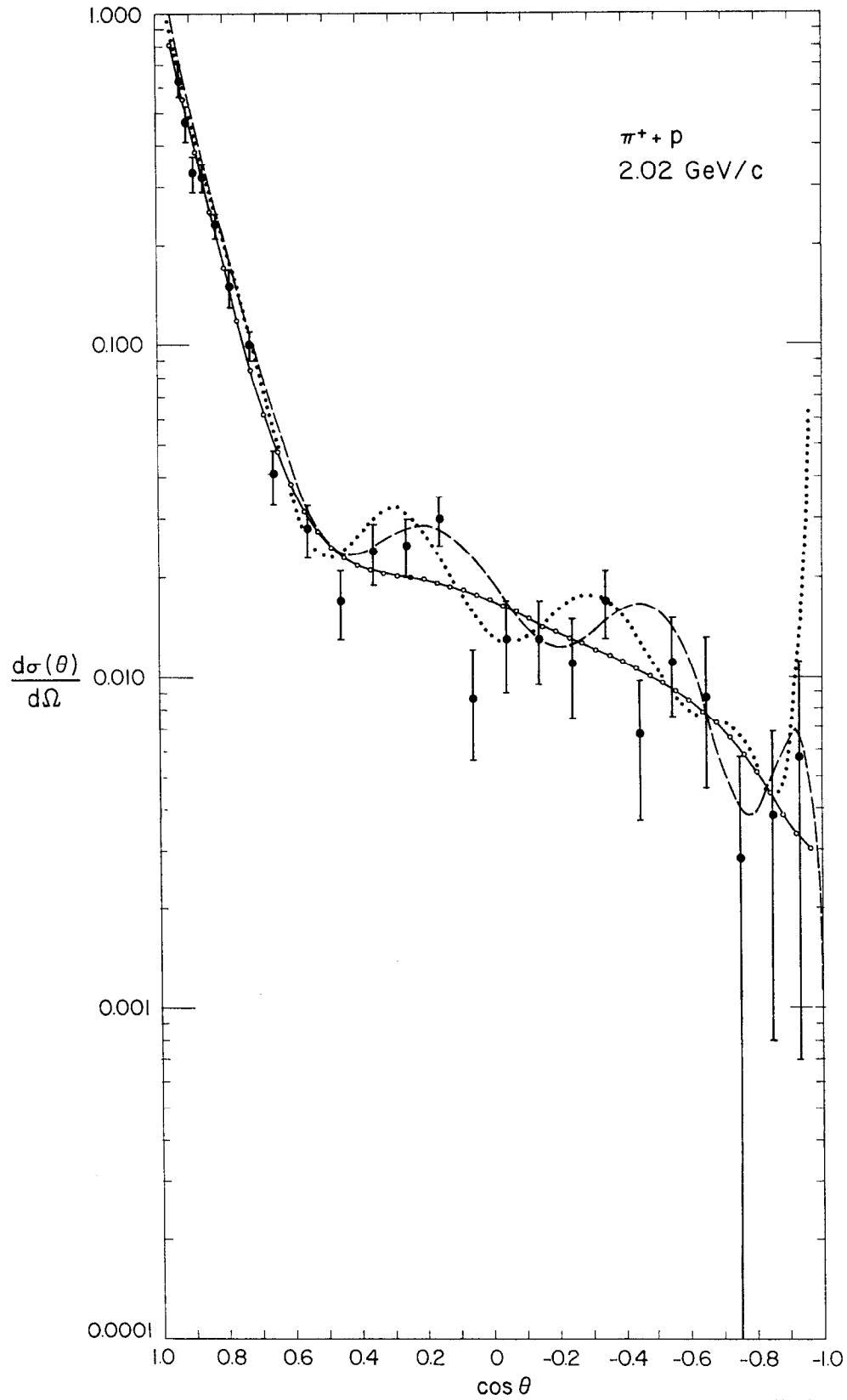


FIG. 2 e

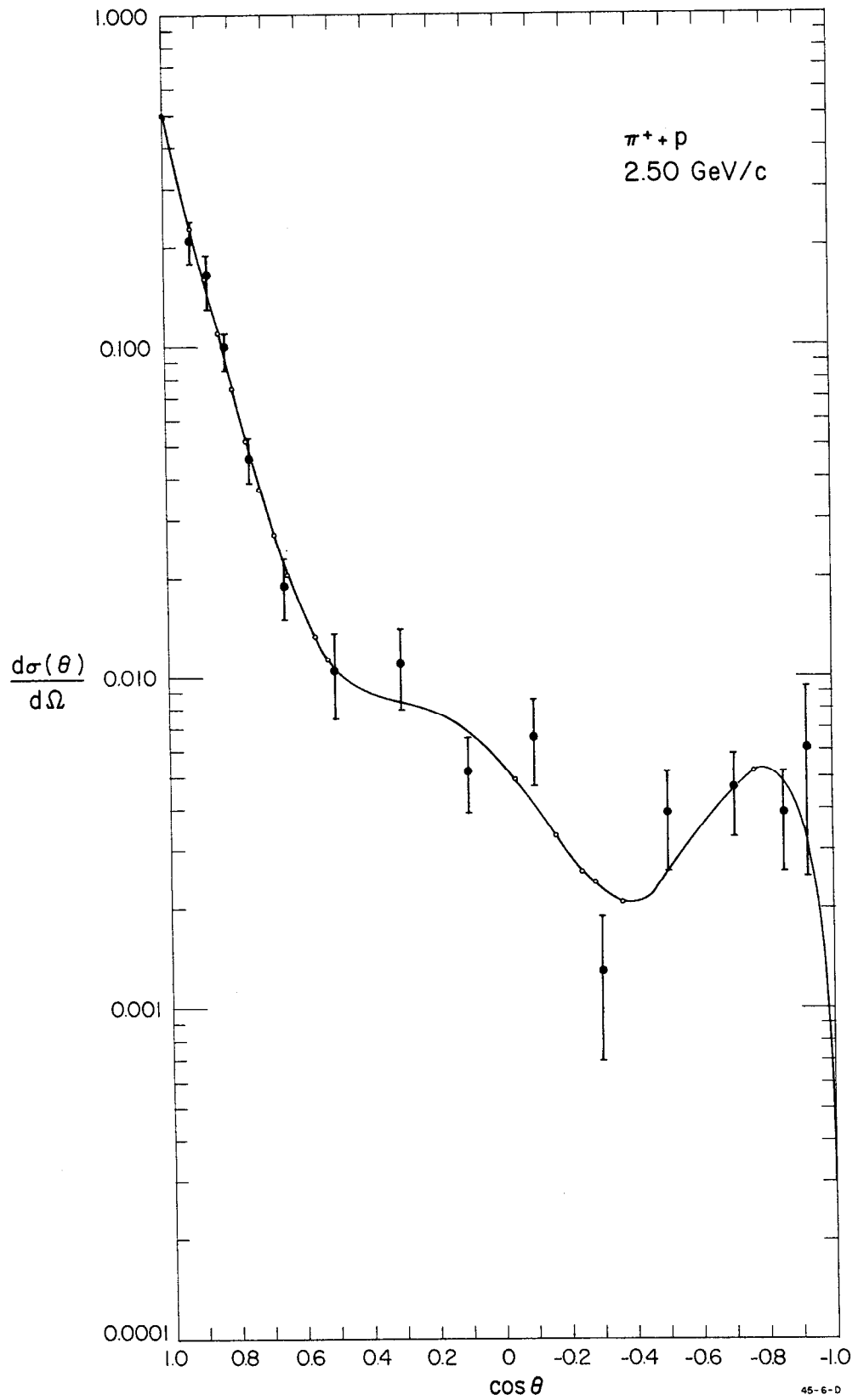


FIG. 2 f

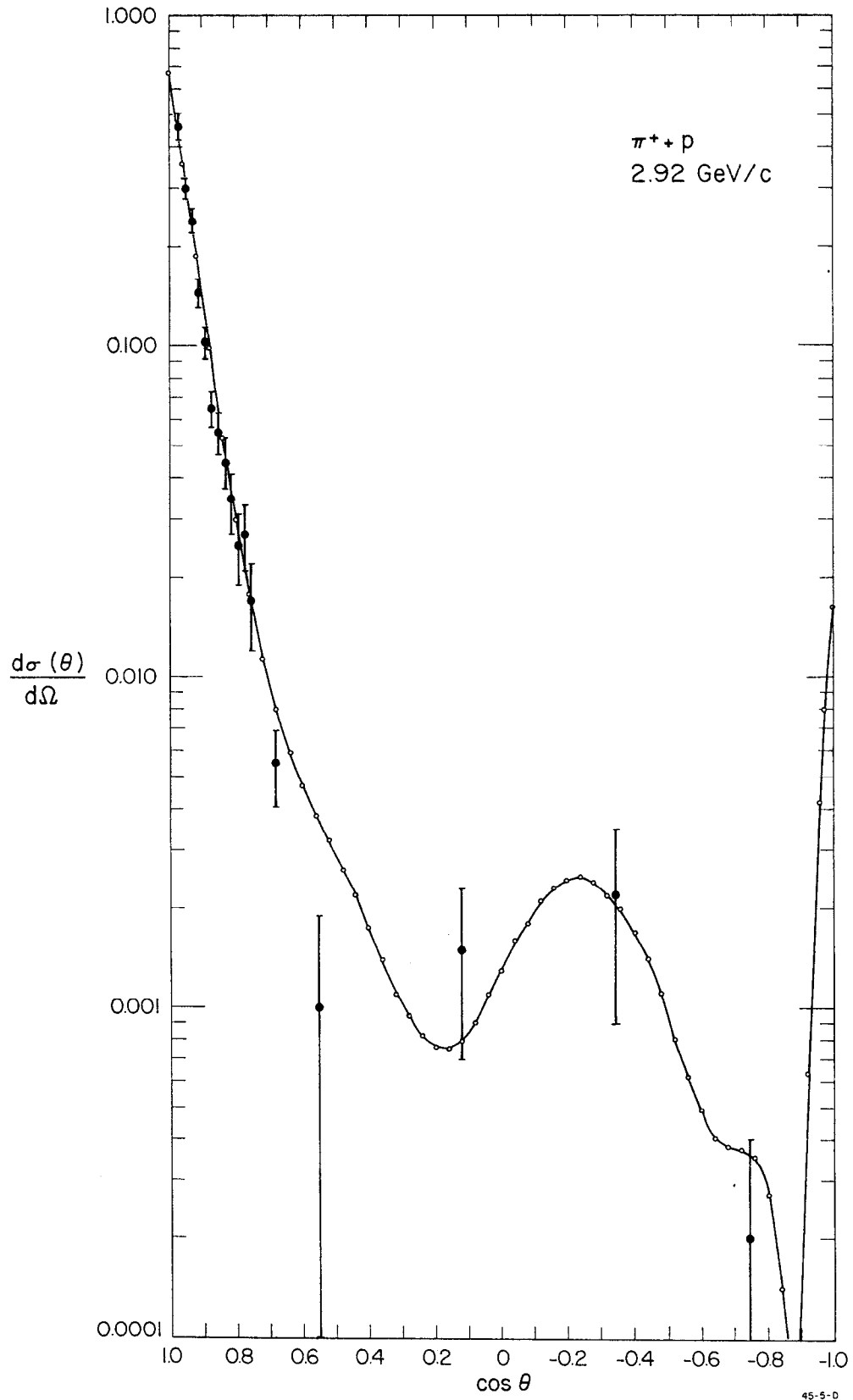


FIG. 2g

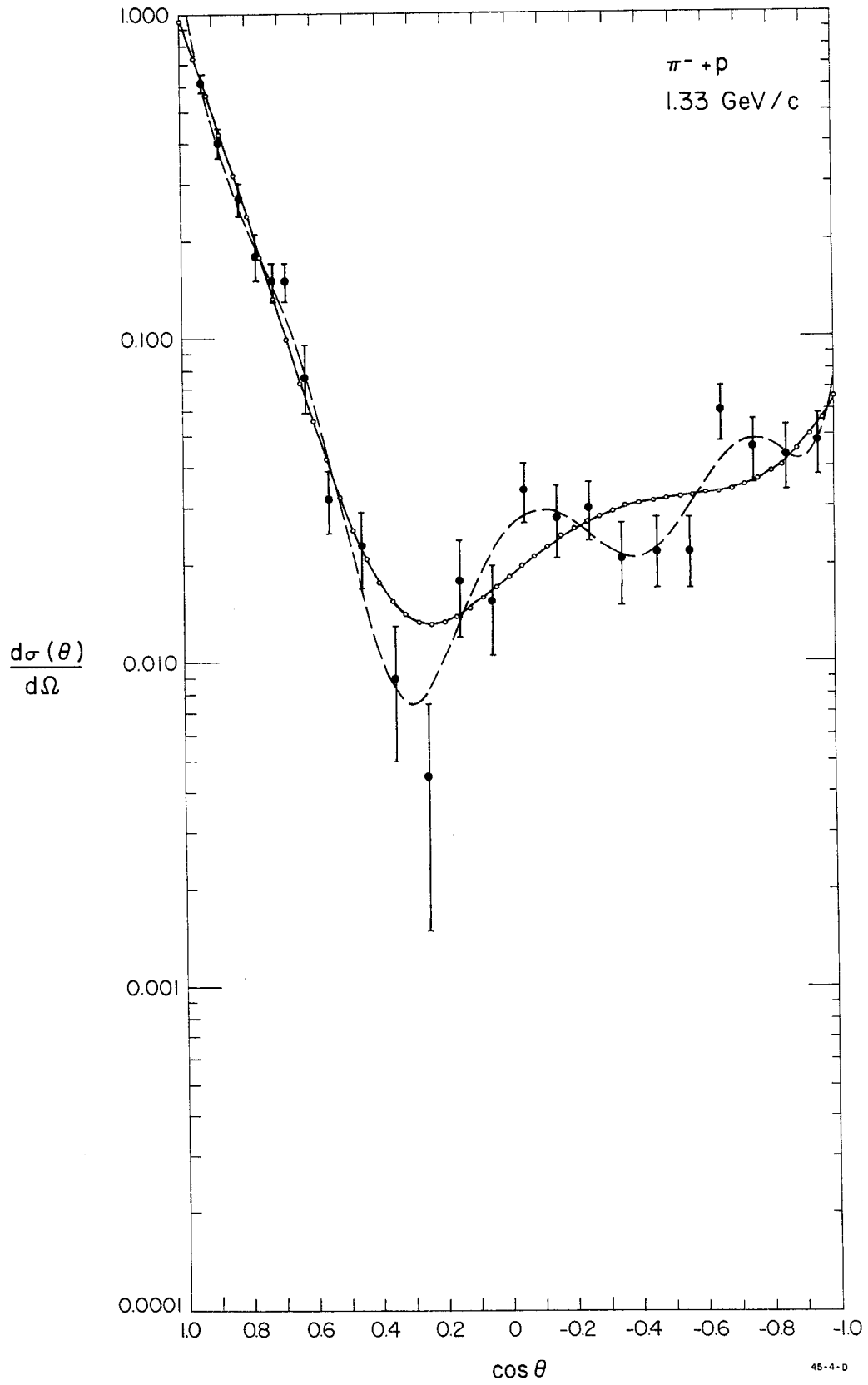


FIG. 3a

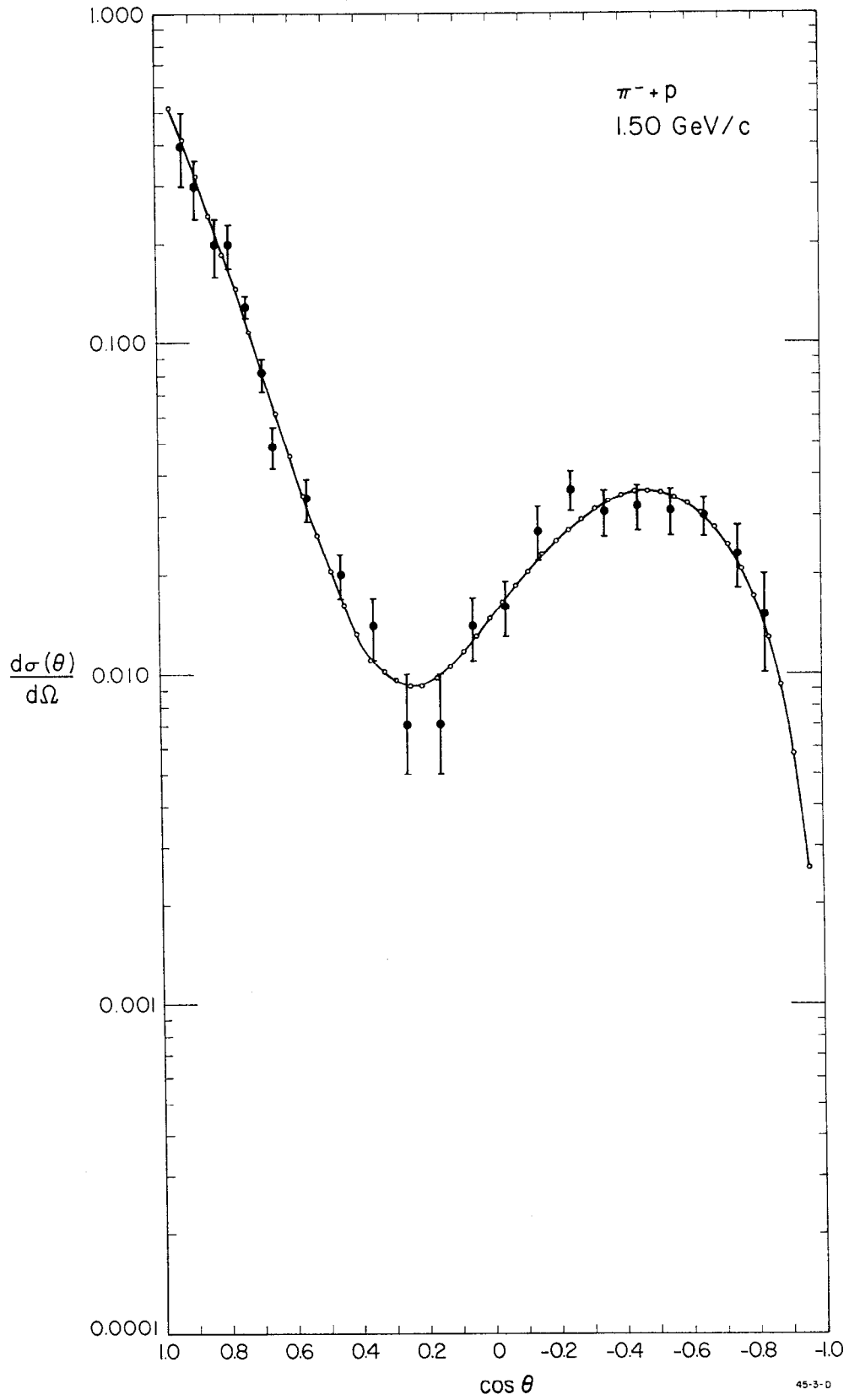


FIG. 3 b

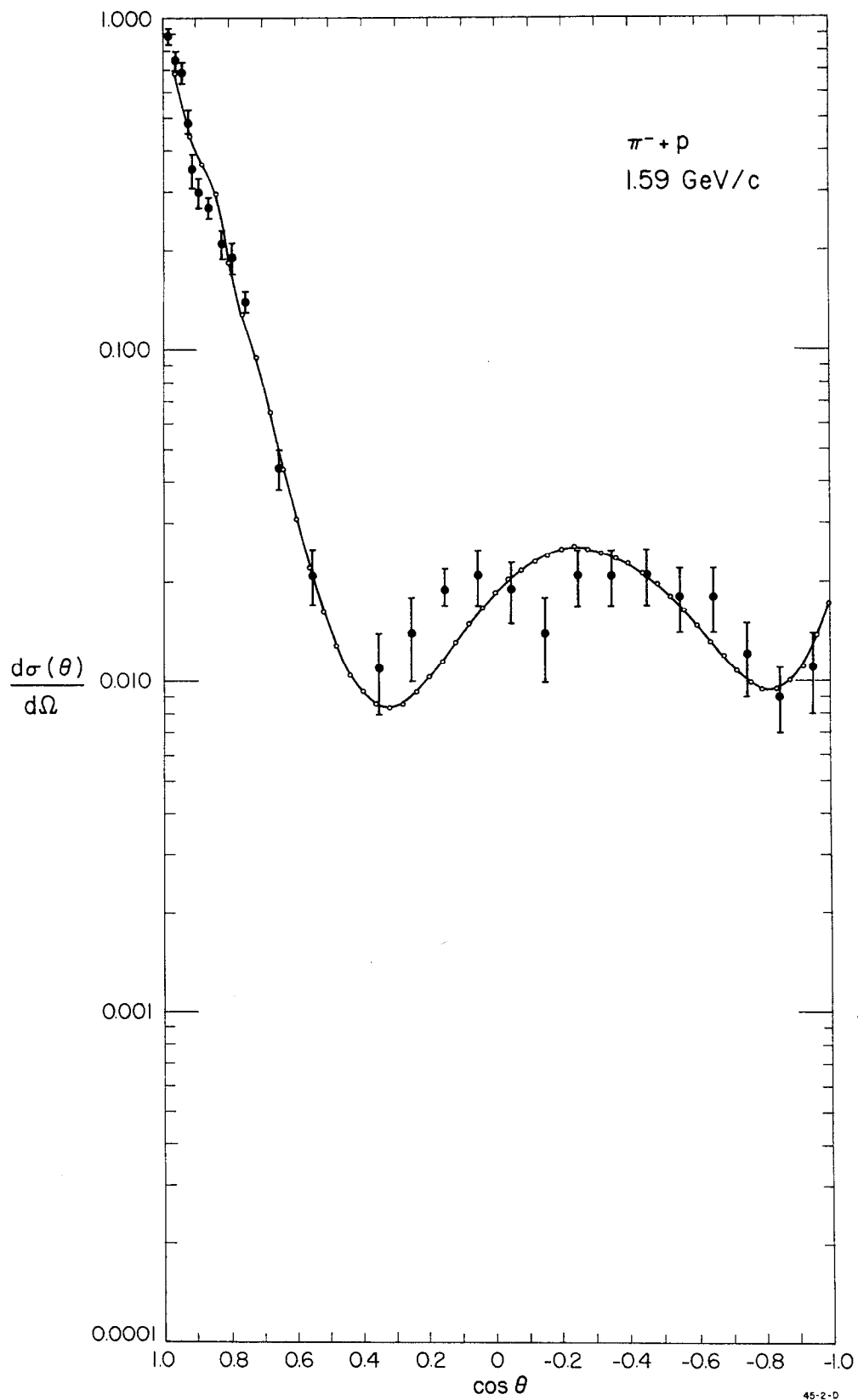


FIG. 3c

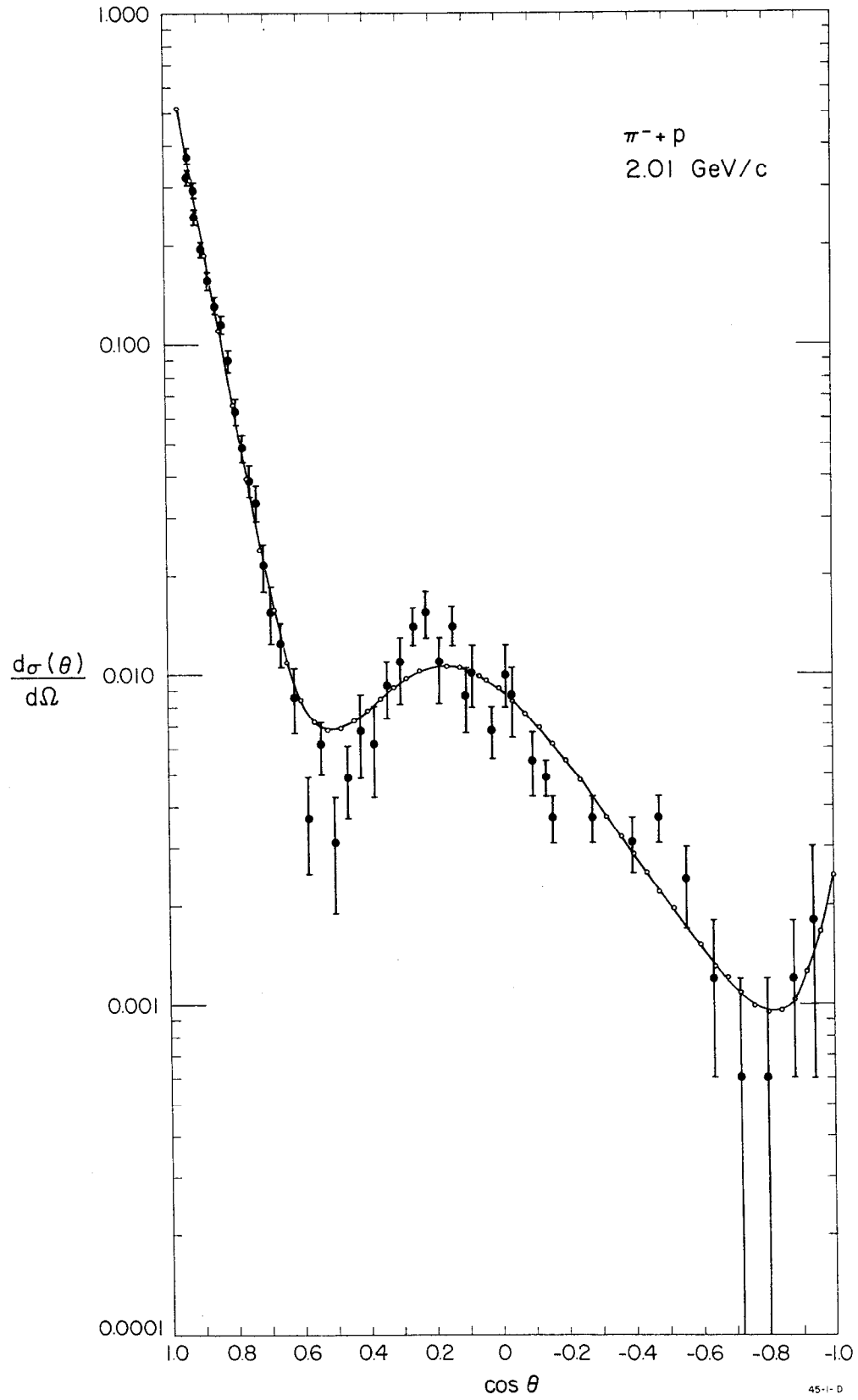


FIG. 3d

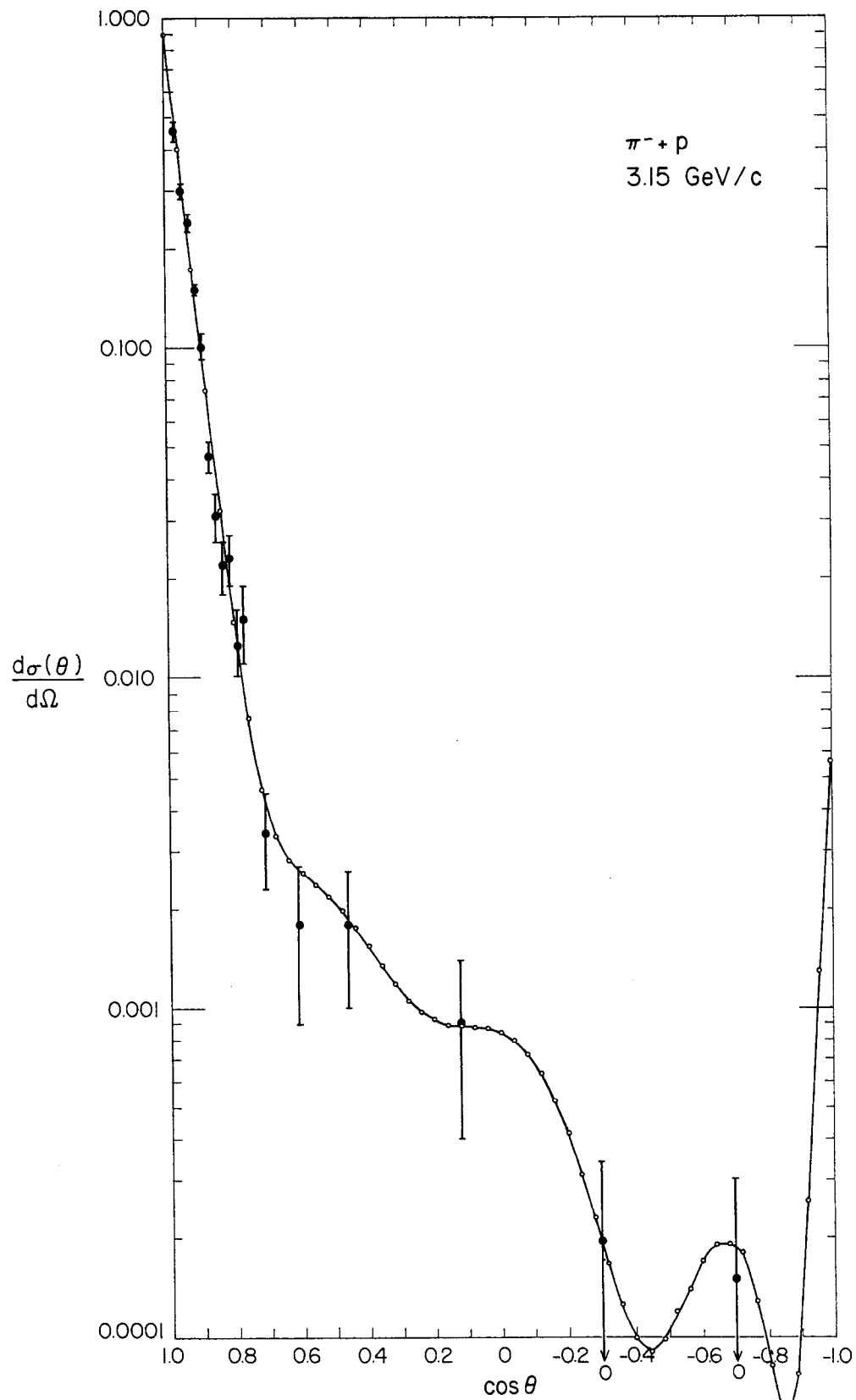
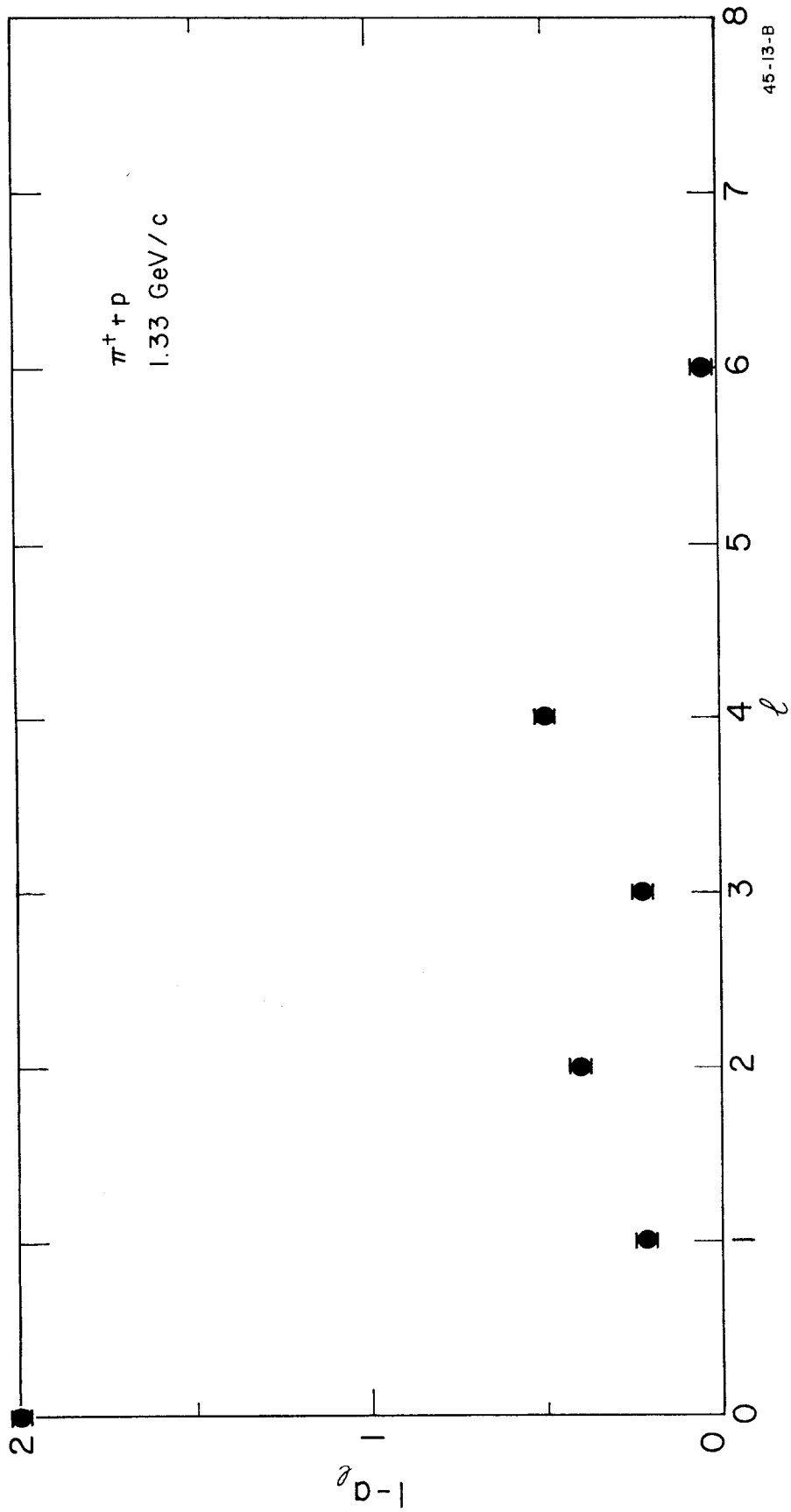


FIG. 3e



45-13-B

FIG. 4 a

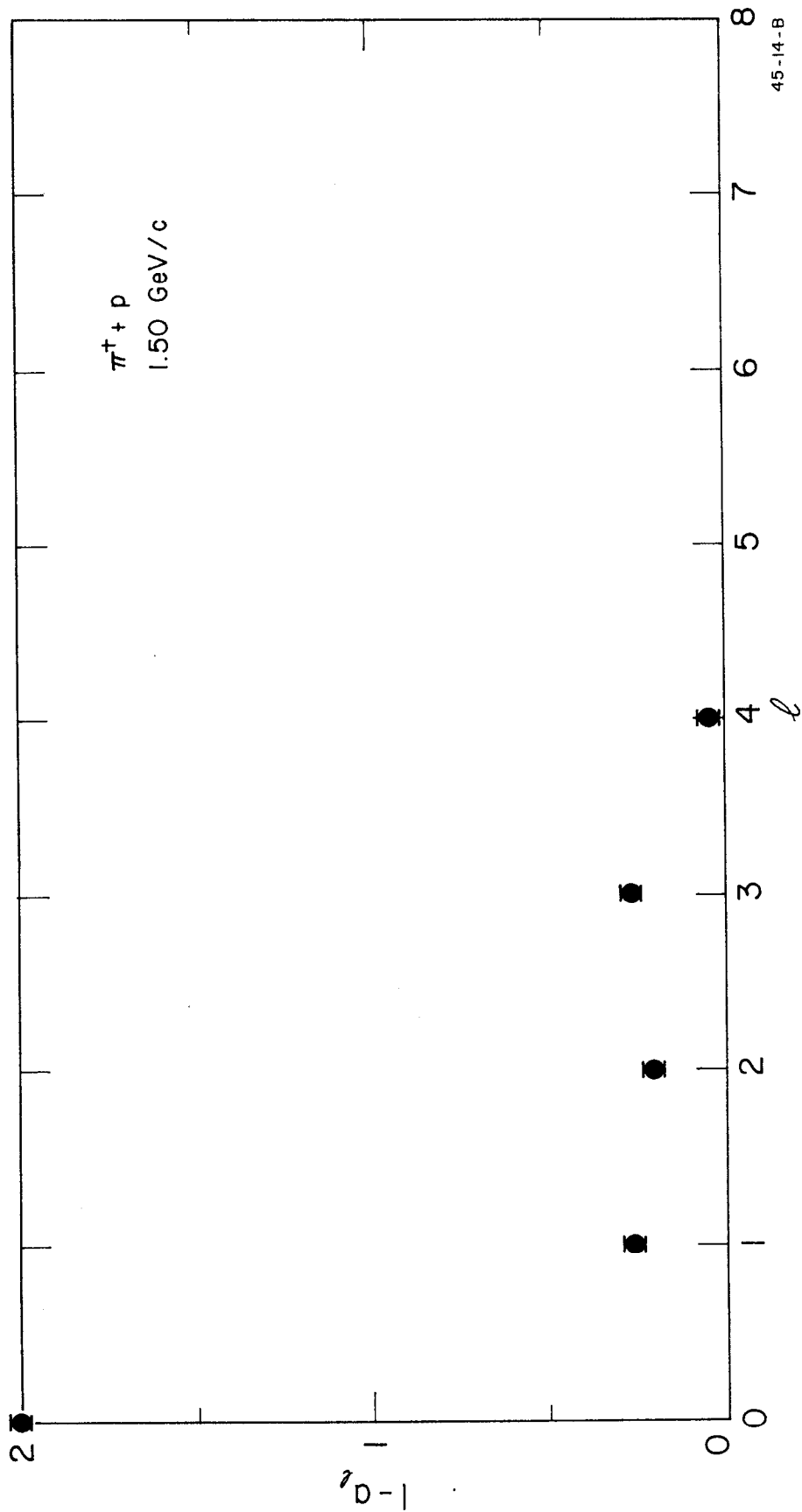
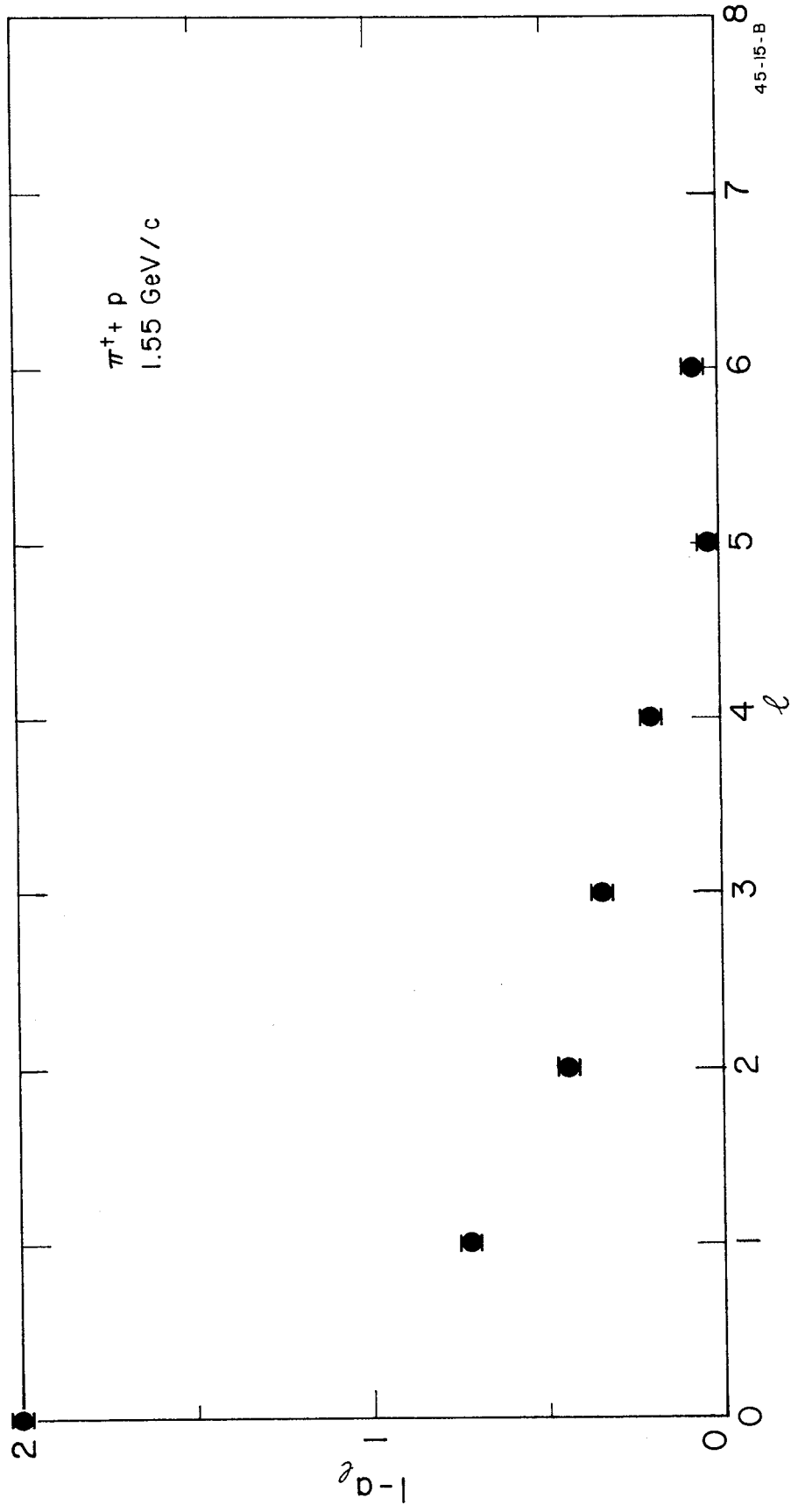
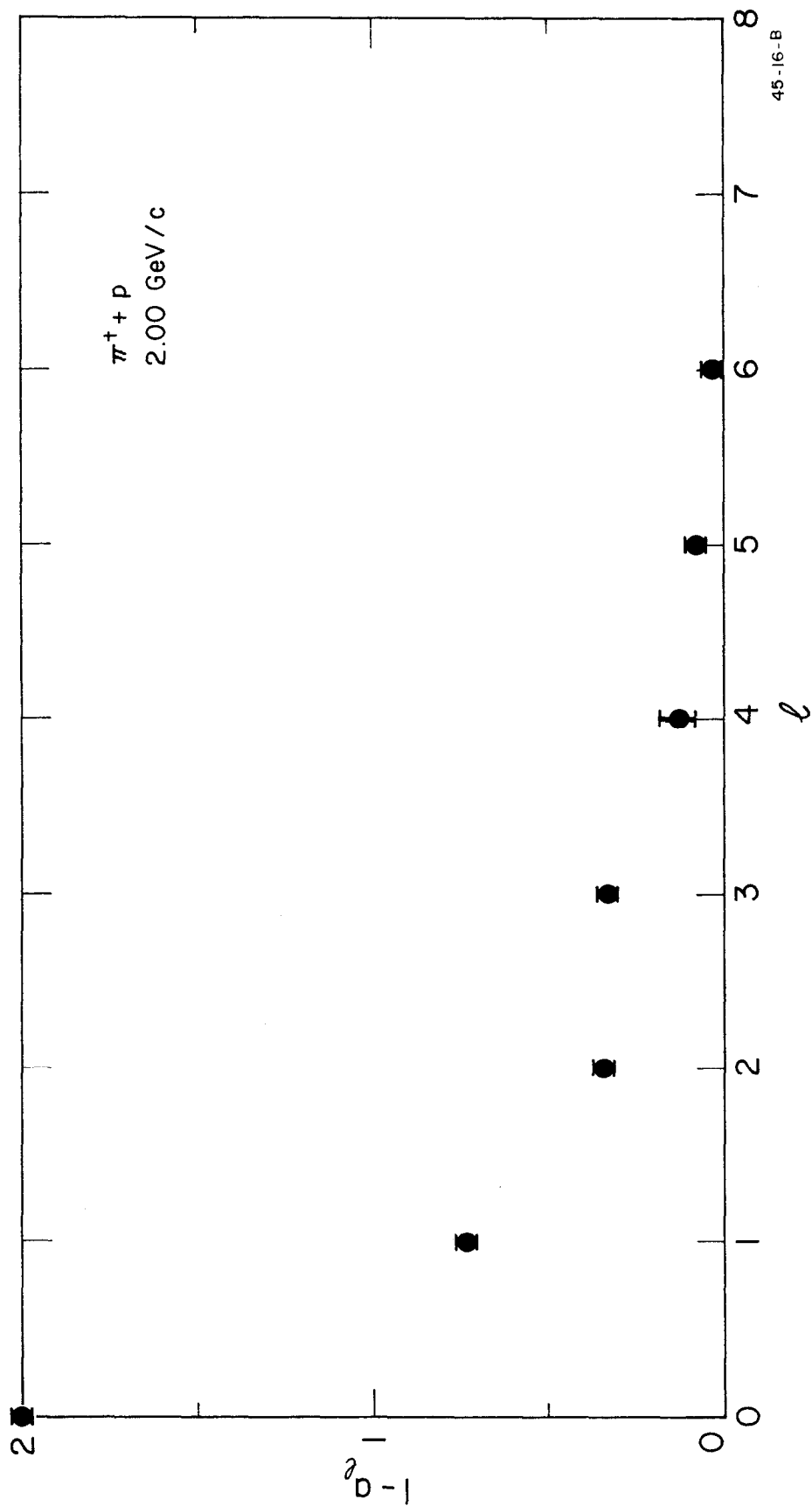


FIG.4b



45-15-B

FIG. 4c



45-16-B

FIG. 4d

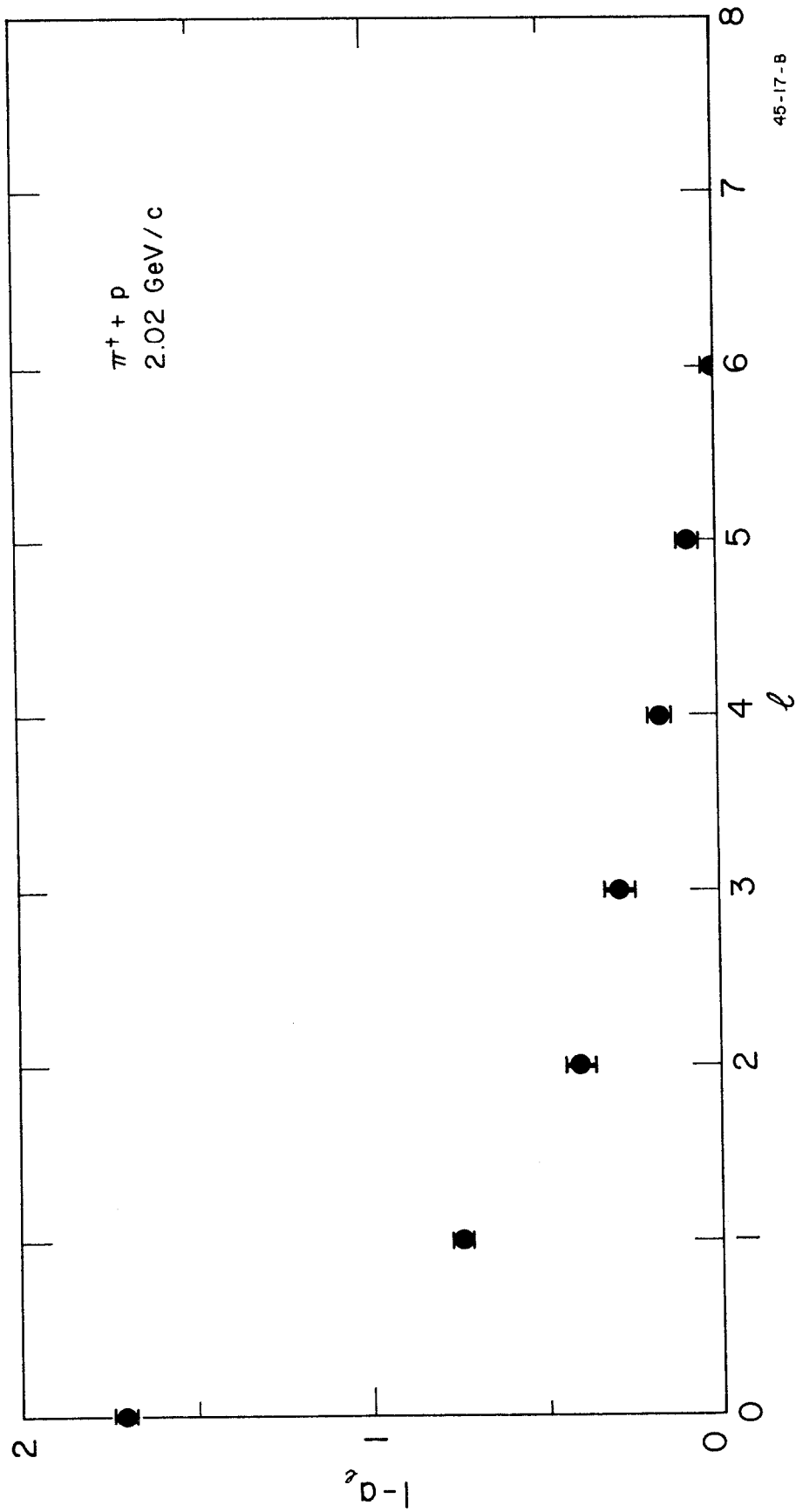


FIG. 4e

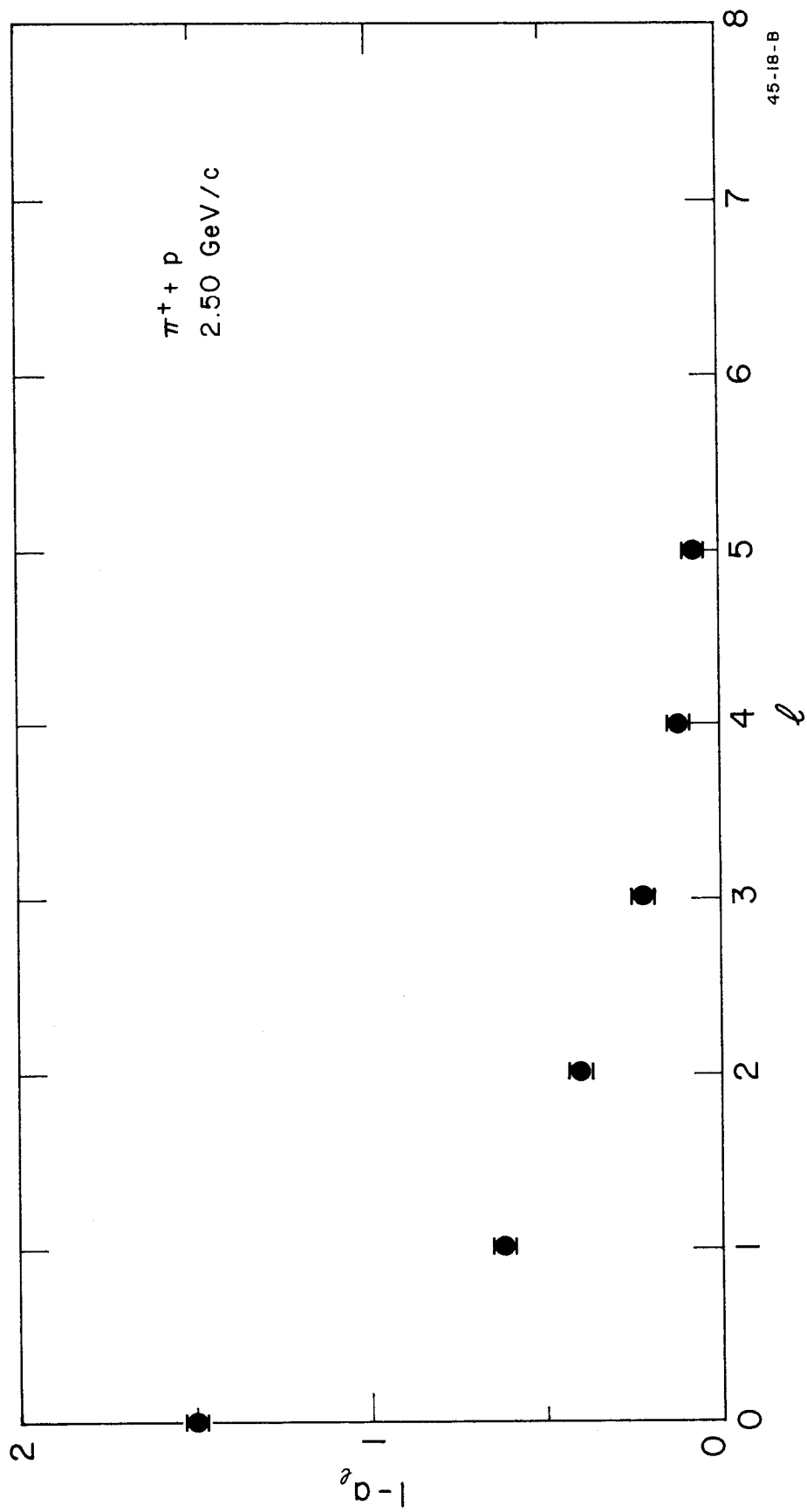


FIG. 4f

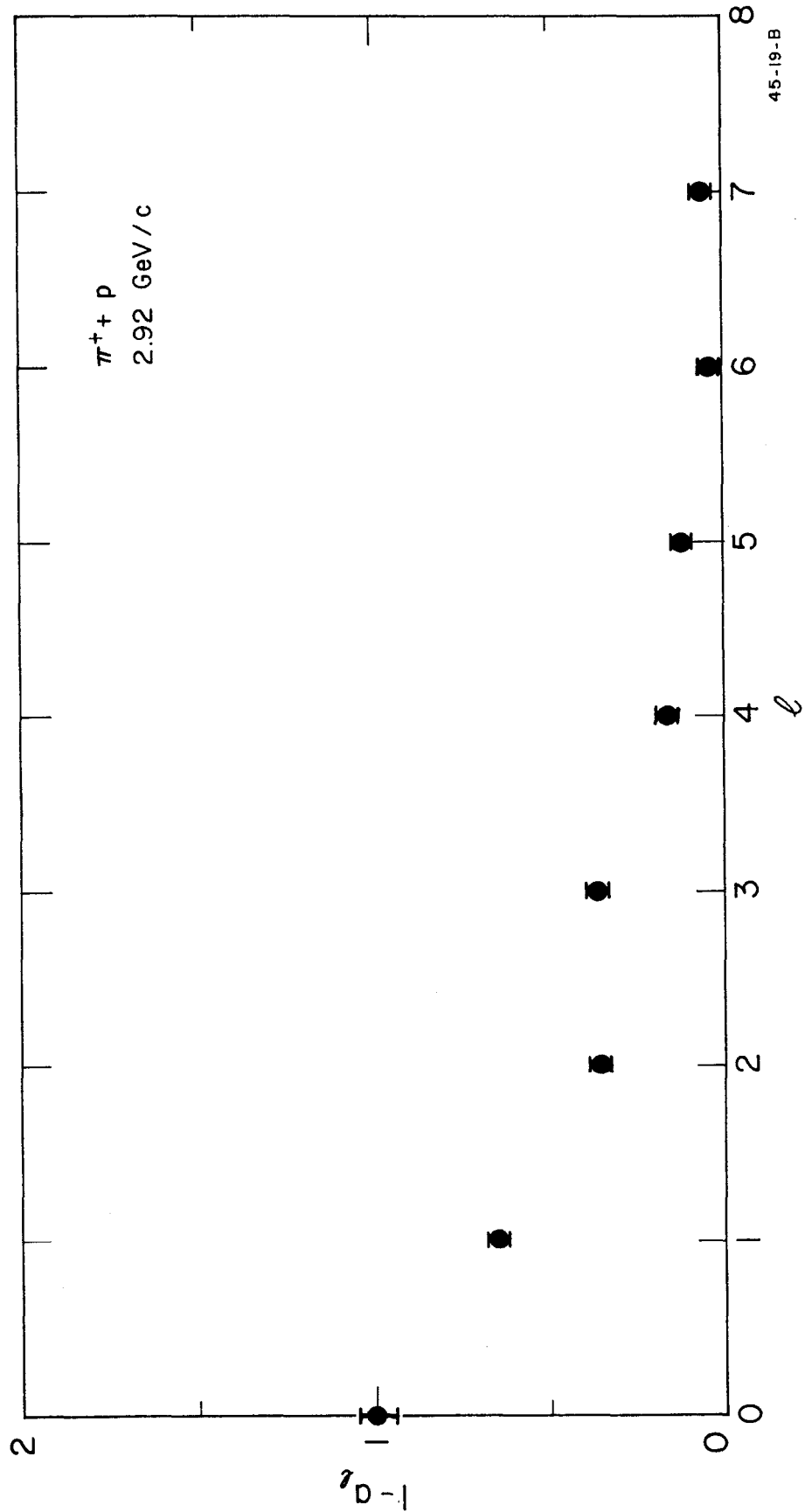
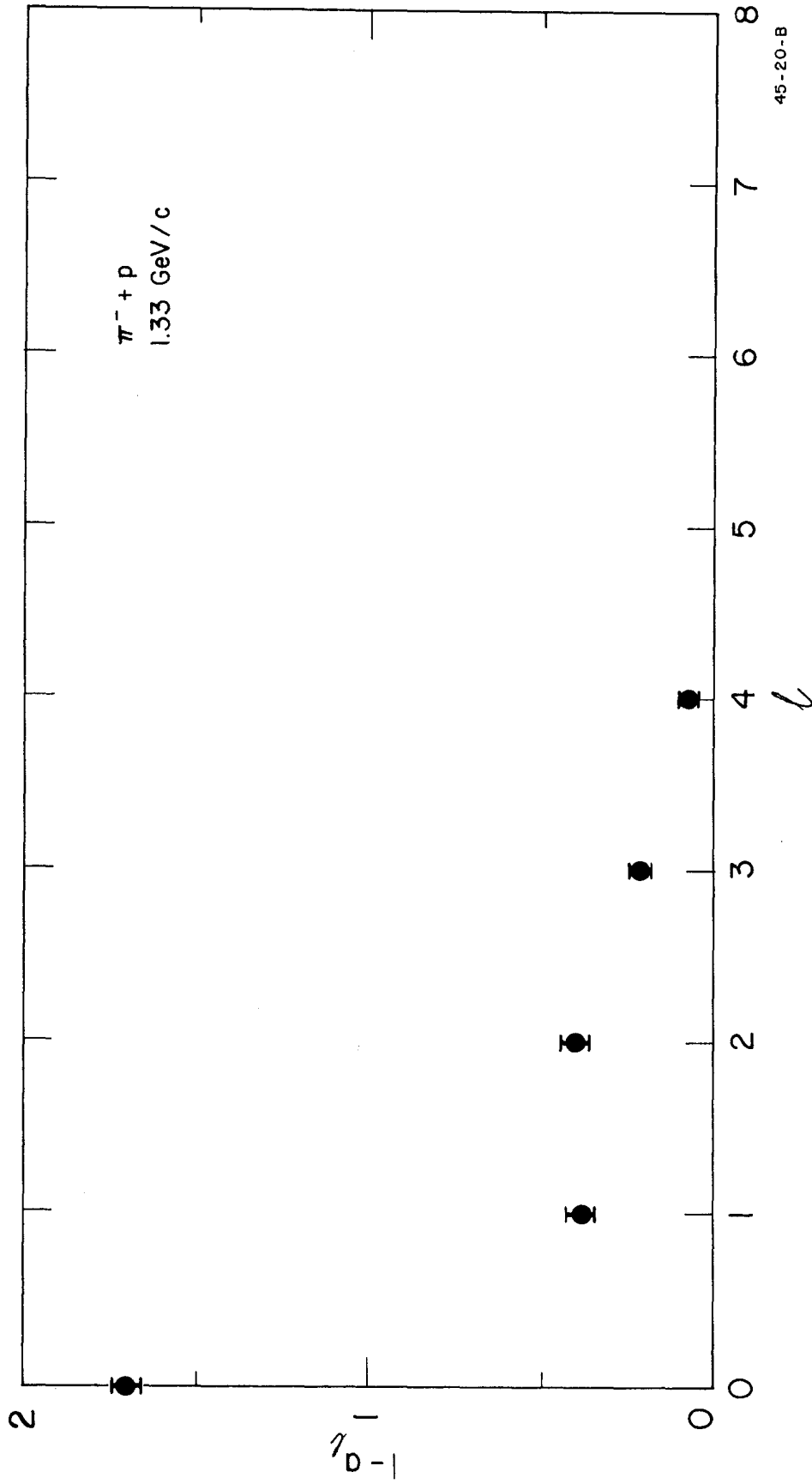
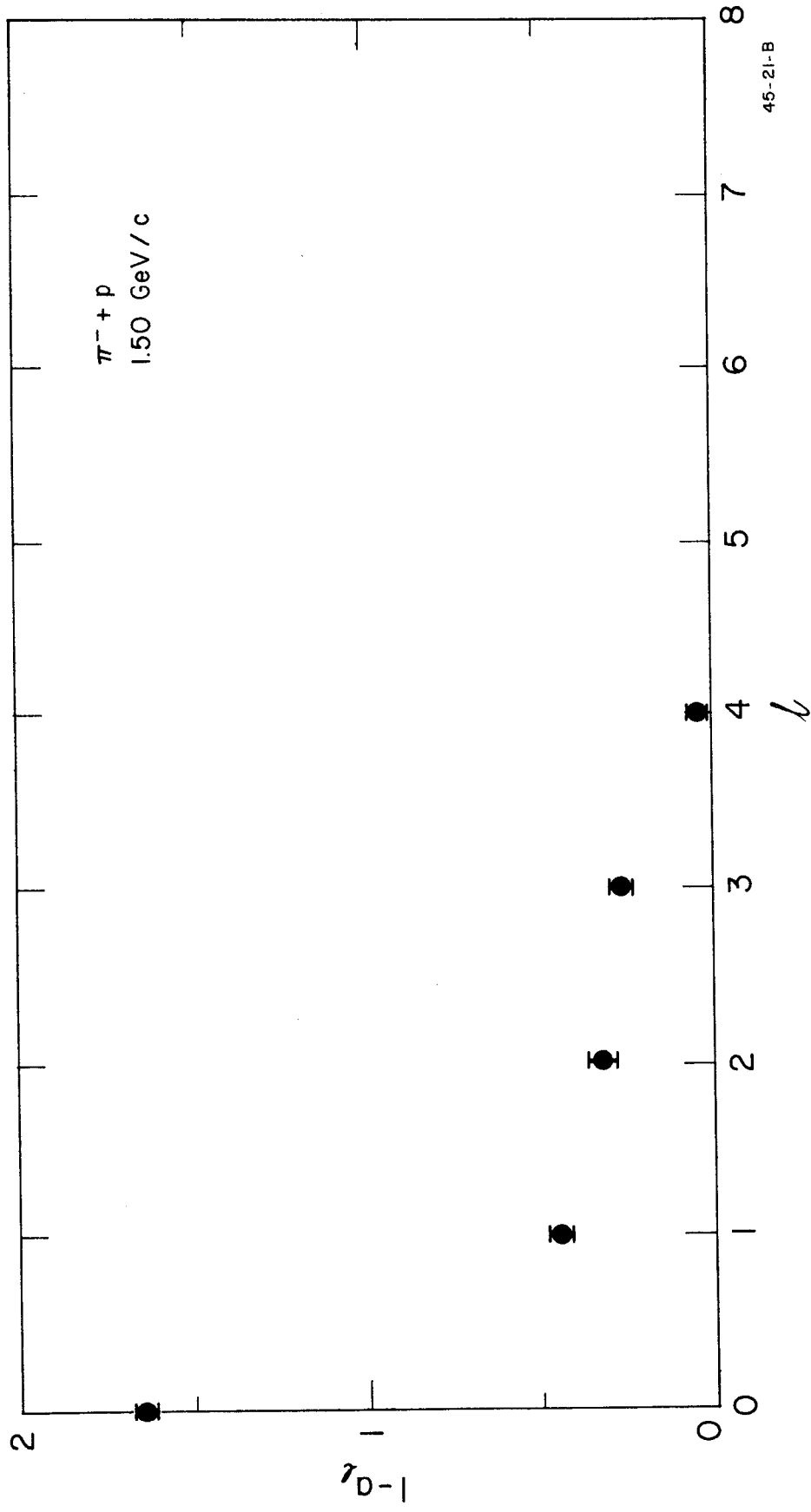


FIG.4g



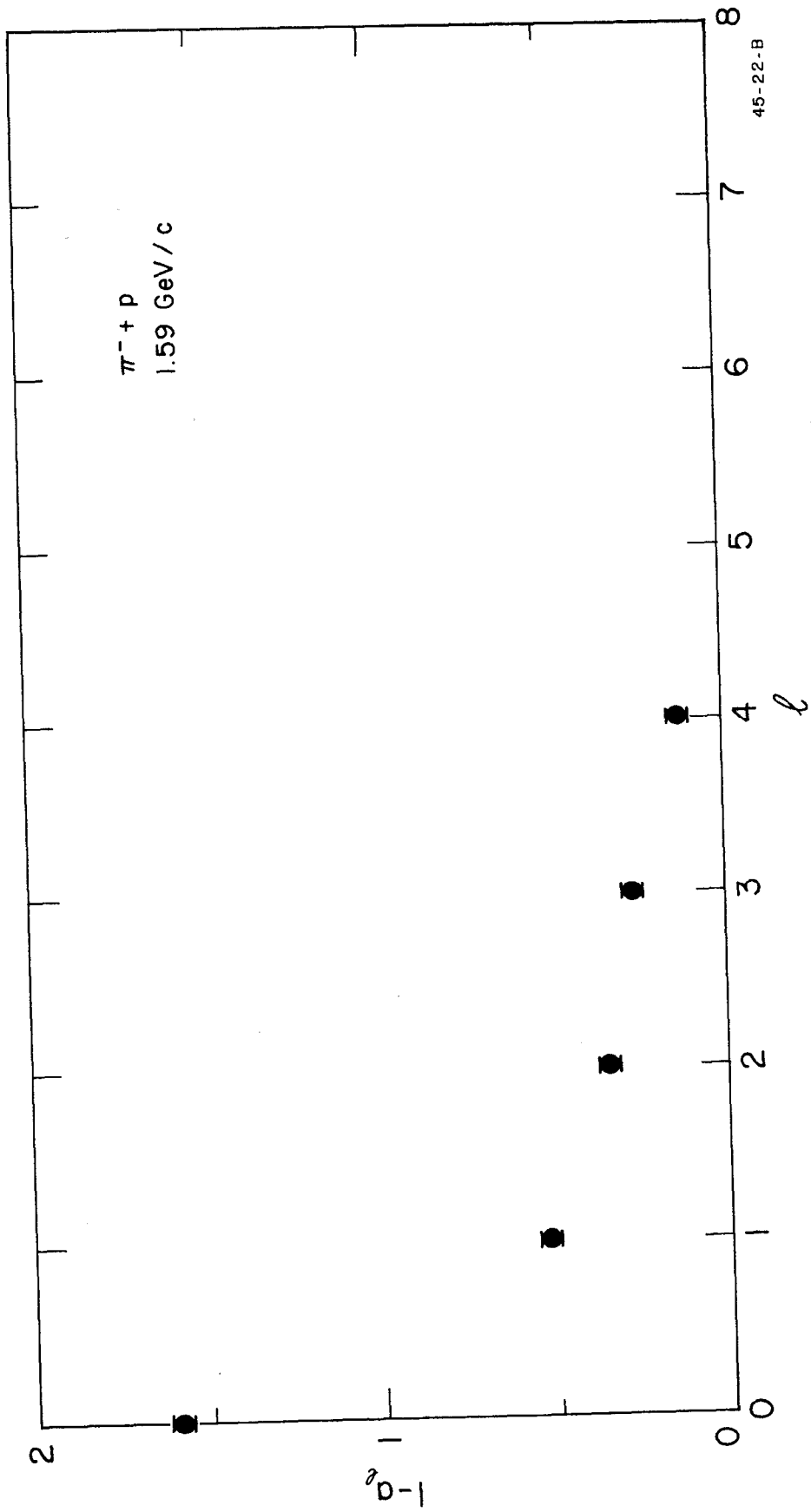
45-20-B

FIG. 5a



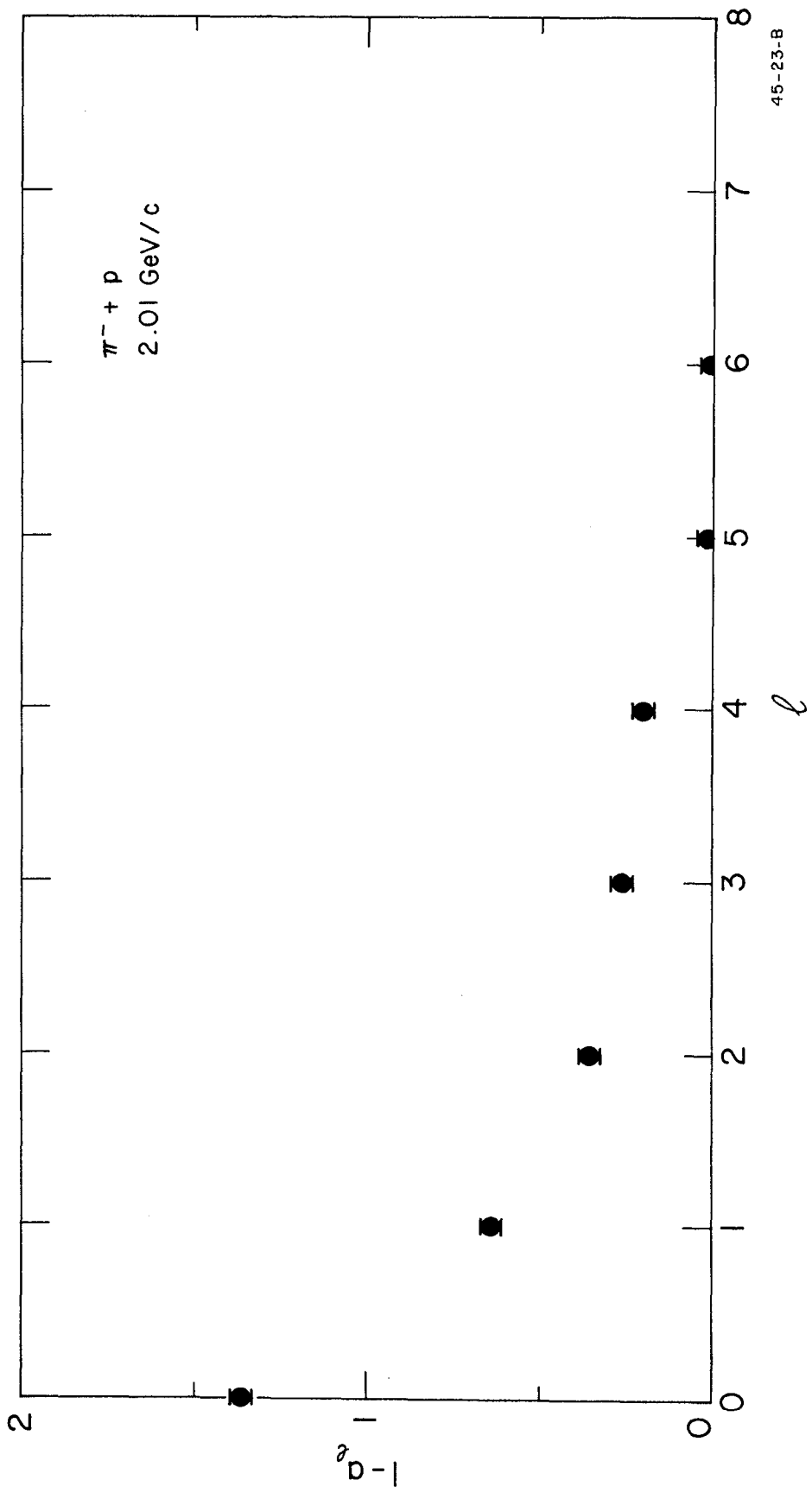
45-21-B

FIG. 5b



45-22-B

FIG.5c



45-23-B

FIG.5d

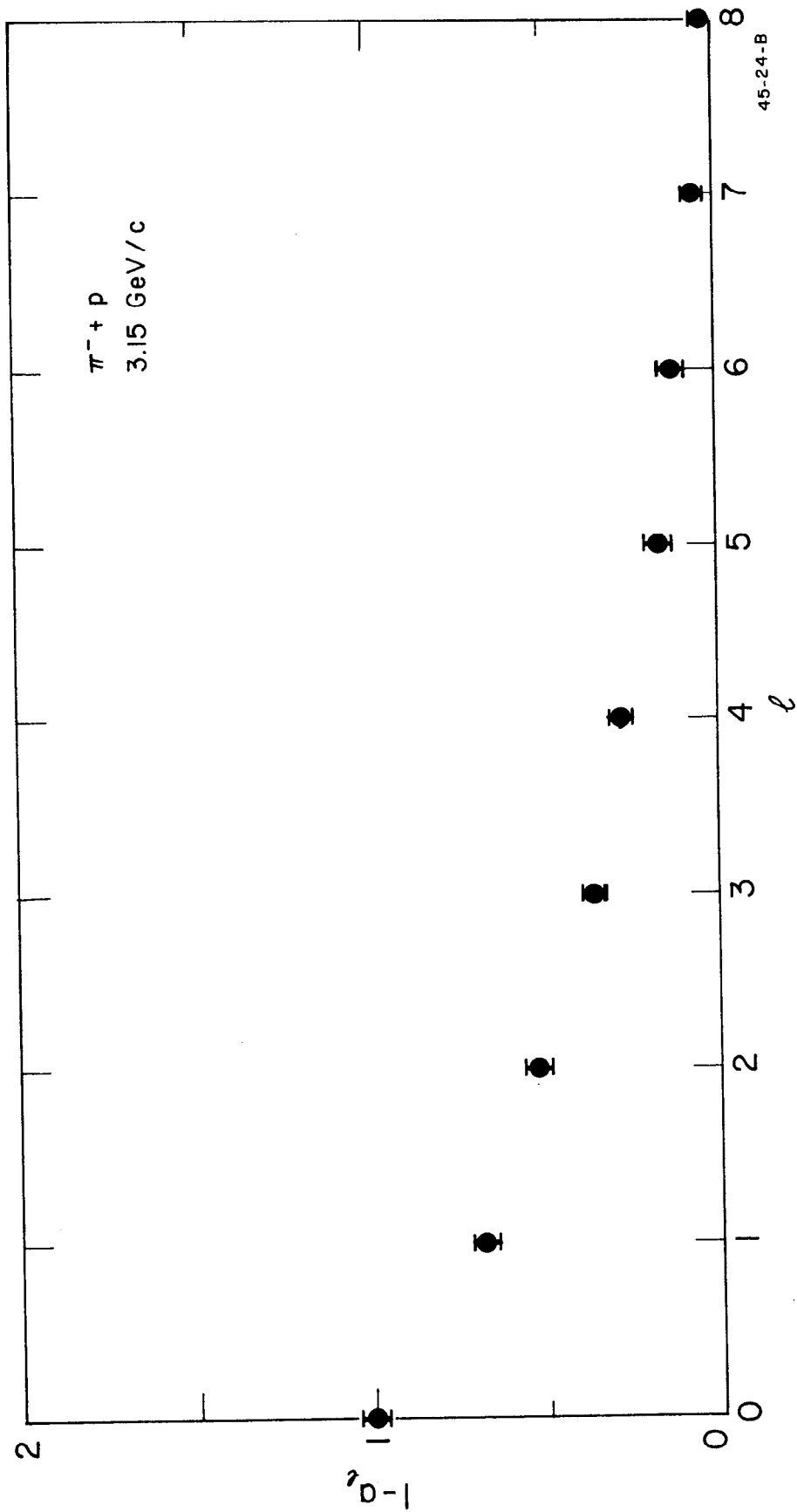
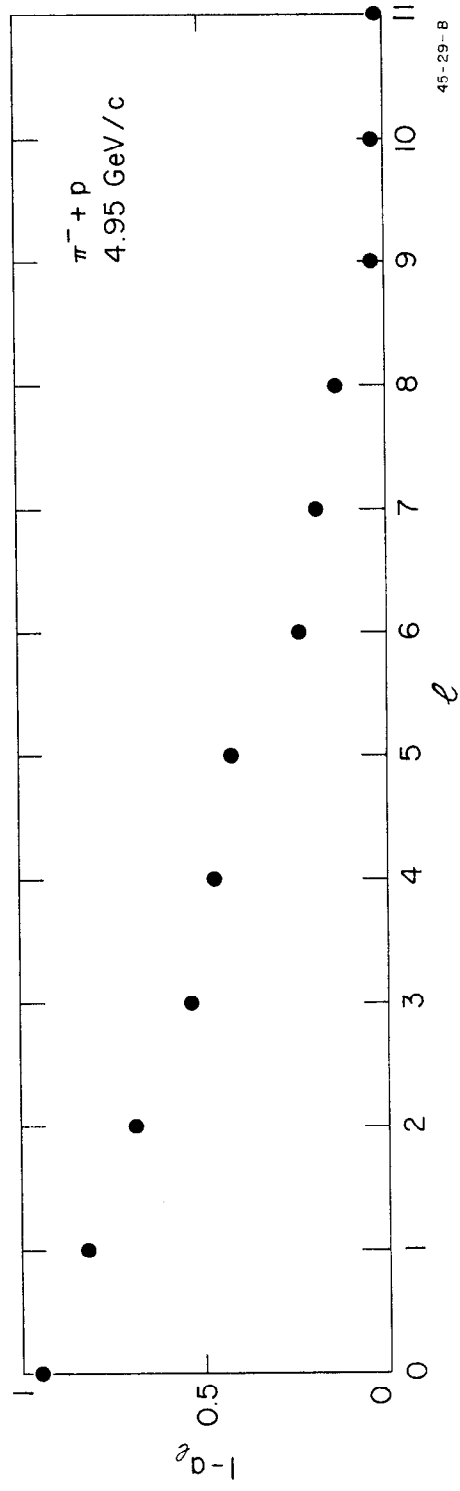
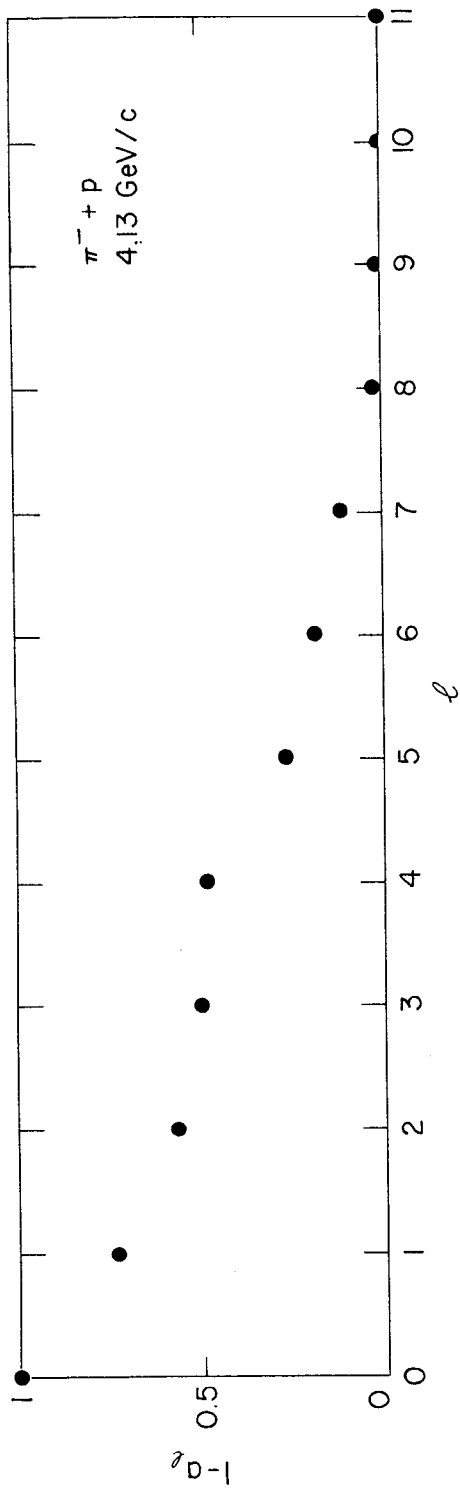


FIG.5e



45-29-B

FIG. 6

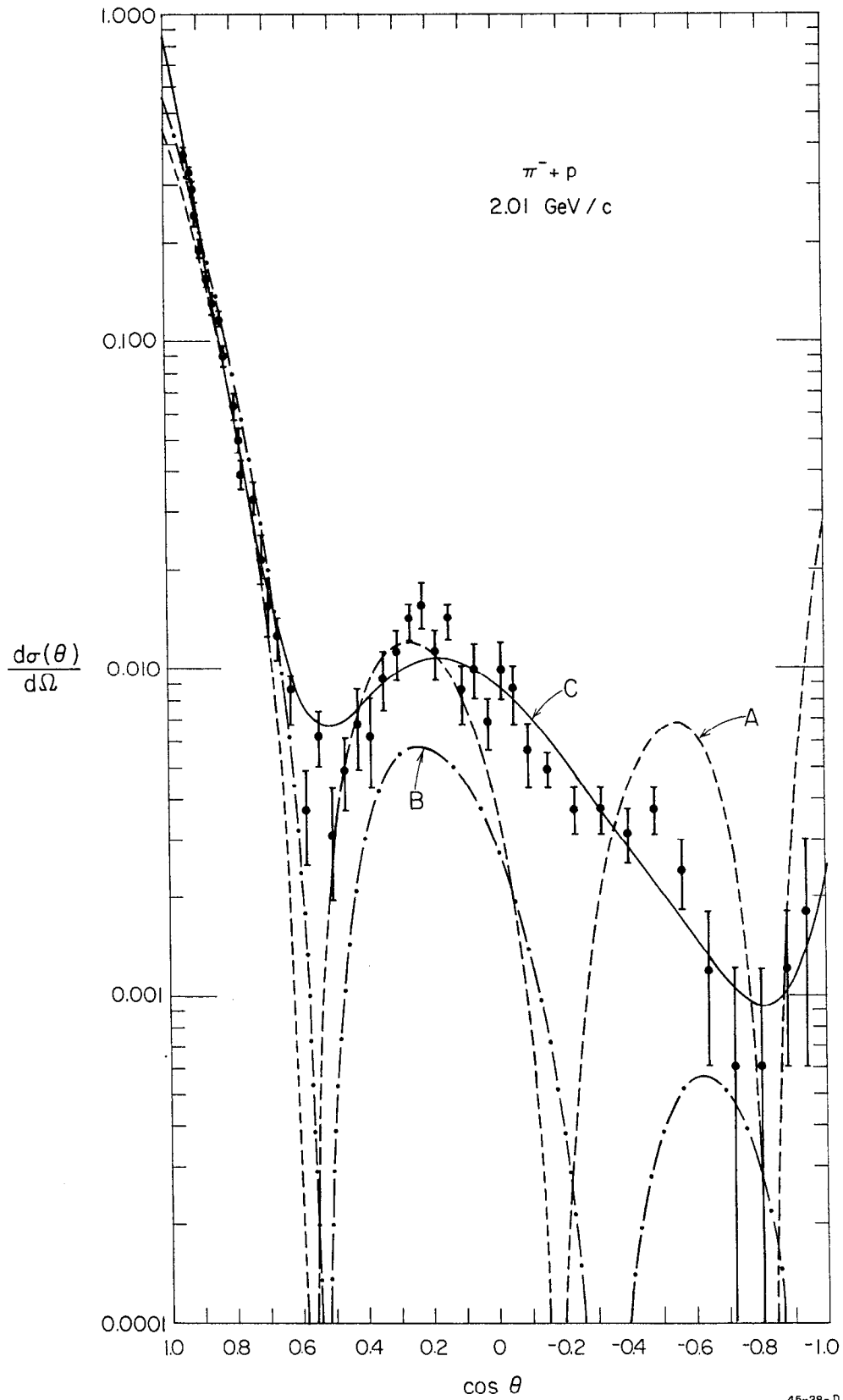


FIG. 7a

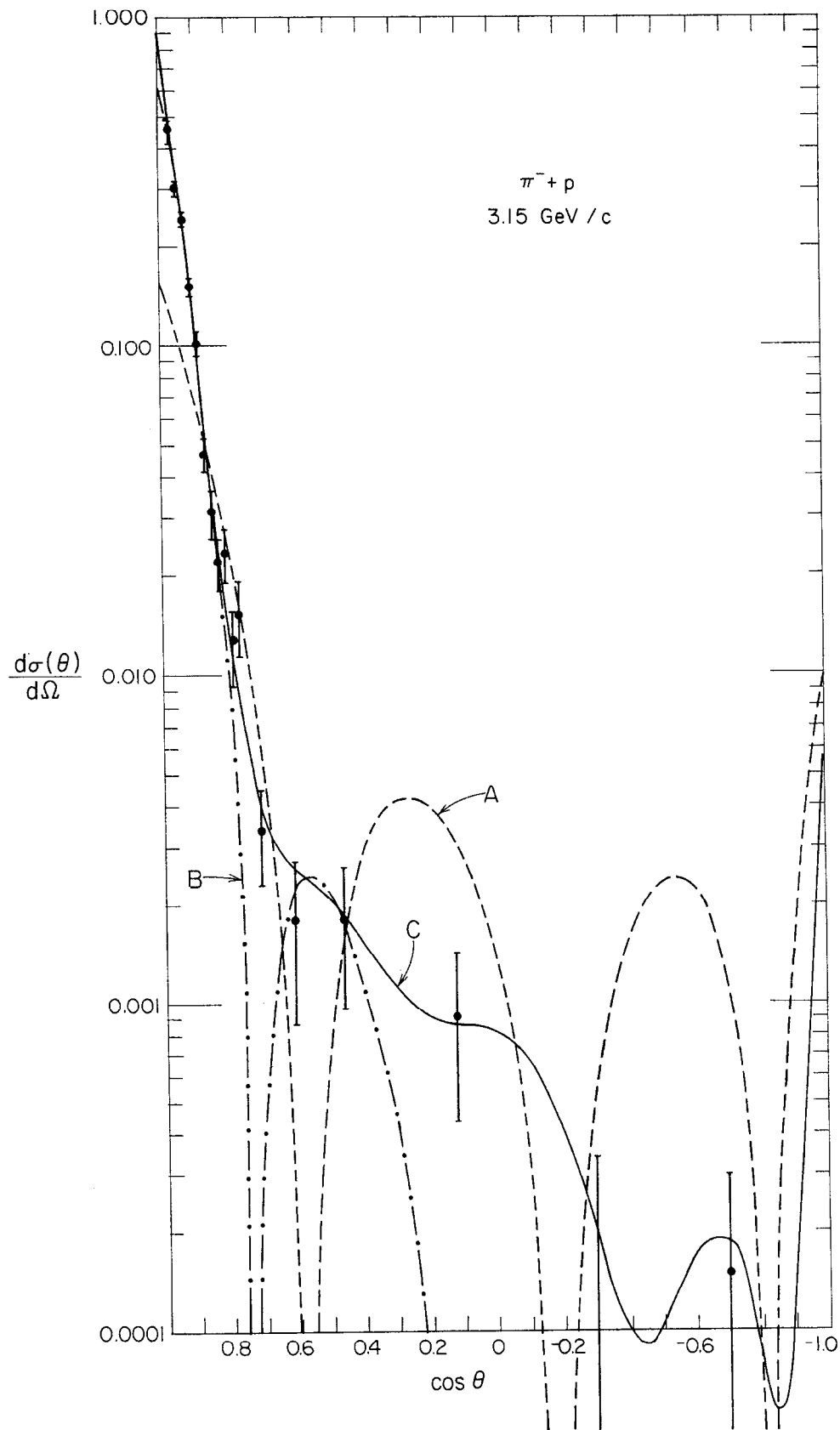


FIG. 7b

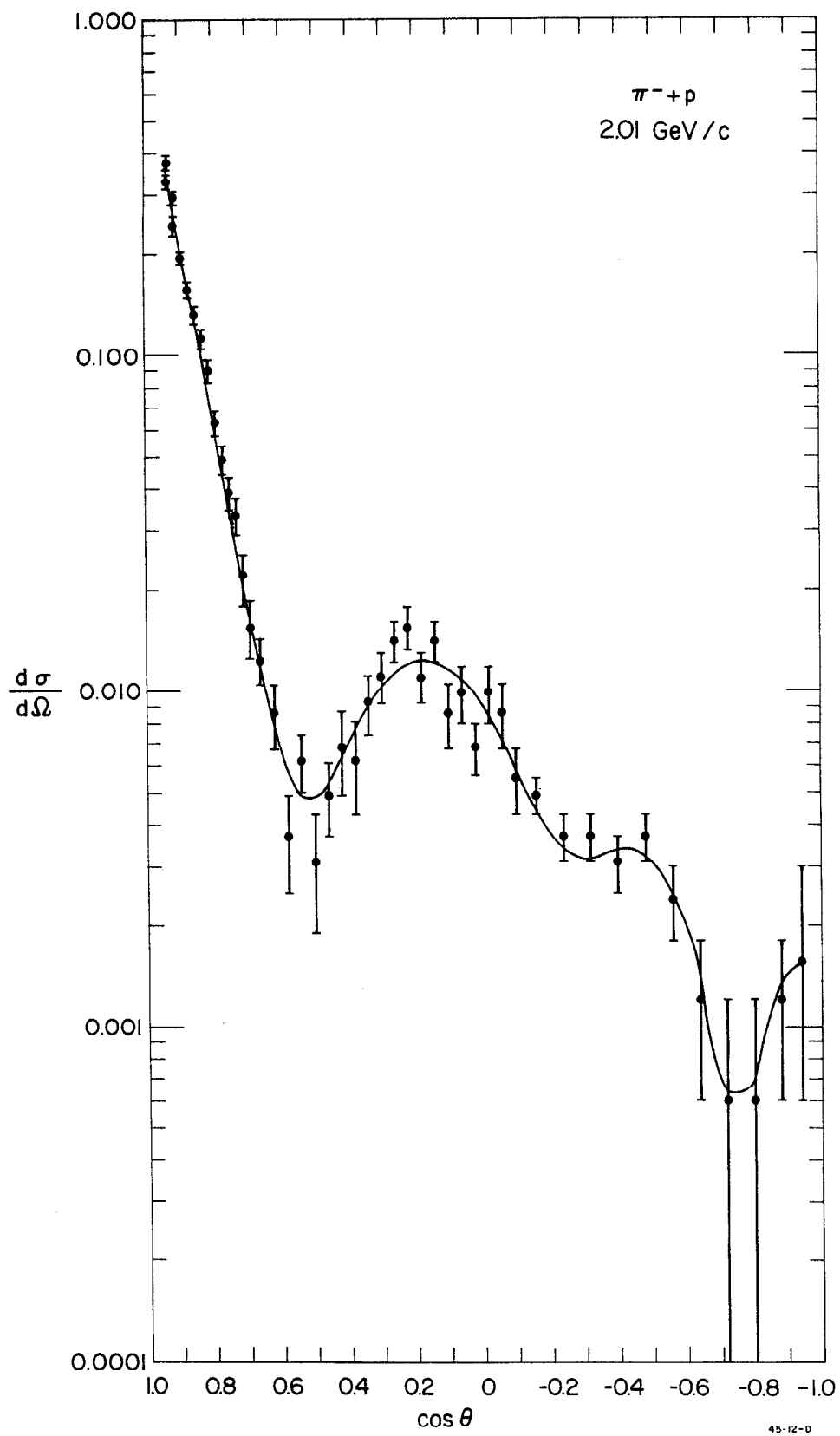


FIG. 8